

**SURFACE CIRCULATION AND LATERAL DISPERSION IN THE MONA PASSAGE
AND OFF SOUTHWESTERN PUERTO RICO**

By

Estefanía Quiñones Meléndez

A thesis submitted in partial fulfillment of the requirements for the degree of

MASTER OF SCIENCE
in
MARINE SCIENCES
PHYSICAL OCEANOGRAPHY

UNIVERSITY OF PUERTO RICO
MAYAGÜEZ CAMPUS

2018

Approved by:

Aurelio Mercado Irizarry, MS
Member, Graduate Committee

Date

Sylvia B. Rodríguez Abudo, PhD
Member, Graduate Committee

Date

Jorge E. Capella, PhD
Member, Graduate Committee

Date

Miguel F. Canals Silander, PhD
President, Graduate Committee

Date

Luis D. Aponte, PhD
Representative of Graduate School

Date

Ernesto Otero Morales, PhD
Chairperson of the Department of Marine Sciences

Date

Abstract

The Mona Passage (MP) is characterized by its complex bathymetry and strong ocean currents forced by tides, winds and baroclinic flows. To understand the impacts of these currents on surface dispersion processes within and around the MP, clusters of GPS-tracked drifters were deployed in early February 2015 and in late April 2017. The 2017 deployment followed the space-filling configuration described by Poje et al. (2014) and denotes the first time that a significant number of clustered drifters (>20) was deployed simultaneously near the MP. The current-following drifters were built in-house following the Coastal Dynamics Experiment (CODE) design introduced by Davis (1985). Drifter velocity observations confirmed the existence of strong, tidally dominated currents modulated by baroclinic processes such as mesoscale eddies and filaments. The wind effect on the drifters was quantified through an inter-comparison between surface current velocity estimates (from the drifters) and observations from high frequency radars. The dispersion dynamics of particles were studied by analyzing drifter movements with respect to the deployment site (absolute dispersion), and with respect to each other (relative dispersion). Relative dispersion was based on initial separation distances ranging from ~ 100 m, for drifter pairs in small triangles (sets of three), to ~ 2 km, for drifter pairs in large triangles (sets of nine). For the two clusters deployed, the scale-dependent relative dispersion rate was found to be very similar for scales smaller than 10 km, and consistent with Richardson's two-thirds law. However, for scales larger than 50 km, both clusters showed different separation rates.

Resumen

El Pasaje de Mona (PM), también conocido como el Canal de la Mona, se caracteriza por su batimetría compleja y fuertes corrientes oceánicas forzadas por mareas, vientos y flujos baroclínicos. Para comprender los impactos de estas corrientes en los procesos de dispersión dentro y alrededor del PM, se desplegaron grupos de cuerpos de deriva rastreados por el Sistema de Posicionamiento Global (GPS, por sus siglas en inglés). Estos instrumentos se desplegaron a principios de febrero de 2015 y a fines de abril de 2017. El despliegue de 2017 siguió la configuración de cobertura de espacio descrita por Poje (et al. 2014) y denota la primera vez que se desplegó, simultáneamente, una cantidad significativa (> 20) de cuerpos de deriva cerca del PM. Los cuerpos de deriva utilizados para este proyecto se caracterizan por su habilidad para seguir las corrientes oceánicas de superficie. Estos instrumentos se construyeron siguiendo el diseño del Experimento de Dinámica Costera (CODE, por sus siglas en inglés) introducido por Davis (1985). Las observaciones de la velocidad de los cuerpos de deriva confirmaron la existencia de corrientes dominadas por mareas moduladas por procesos baroclínicos tales como remolinos y filamentos de mesoescala. El efecto del viento sobre los cuerpos de deriva se cuantificó mediante una intercomparación entre los estimados de la velocidad de corrientes de superficie (provenientes de las trayectorias de los cuerpos de deriva) y las observaciones de los radares de alta frecuencia. La dinámica de dispersión de partículas se estudió analizando los movimientos de los cuerpos de deriva con respecto a su posición de despliegue (dispersión absoluta) y con respecto a la posición de otros cuerpos de deriva (dispersión relativa). La dispersión relativa se basó en las distancias de separación inicial, cuyo rango va desde los ~ 100 metros para triángulos pequeños (conjuntos de tres) hasta los ~ 1 km para triángulos grandes (conjuntos de nueve). Para los dos grupos de cuerpos de deriva, la tasa de dispersión relativa dependiente de la escala resultó ser muy similar a escalas menores de 10 km y consistente con la ley de los dos tercios de Richardson. Sin embargo, a escalas más grandes de 50 km, ambos grupos mostraron tasas de separación diferentes.

© Estefanía Quiñones Meléndez 2018

...to Mom and Dad, for their wholehearted support through this journey of academic and personal growth.

Acknowledgements

Special thanks to my thesis advisor, Miguel Canals, for his intellectual guidance, comforting discussions about life in academia and material support for the past three years. To the other members of my committee: Jorge Capella, Aurelio Mercado and Sylvia Rodríguez, for their constructive criticism. Specially, to Capella for his valuable input regarding many technical aspects of this research. Additional thanks to Graciela García and the Caribbean Fishery Management Council (CFMC) for providing the necessary support to make this project possible.

To my parents, Maricelli Meléndez and Javier Quiñones, for their unconditional love and support. My most sincere thanks are given to them, to my grandparents, and to my sisters. Without all of them as a source of constant motivation, this work would not have been possible.

To David Carrero, Patricia Chardón, Luis Pomales, Joan Bonilla, and Emmanuel Colón for providing invaluable help with the design development of the drifter, its construction, the experimental setup, and the field deployments. To Colin W. Evans for providing **Fig. 4.6** and the data access tools used for **Section 4.2.1**. To Juan González for developing the original analytical tools for data in **Section 4.2.1**. To Esteban López for digitalizing the drifter blueprints.

To friends at the Center for Applied Ocean Science and Engineering, and at the Department of Marine Sciences, for sharing their knowledge and friendship with me: Gabriela Salgado, Fabián García, Adail Rivera, Carlos García, Natalia Ramirez, and Christian Rojas. Special thanks to my close friends: Paola, Camila, Alexandra and Ivana for all their encouragement over the past years.

This study was supported by the CFMC (NOAA Coral Reef Conservation Program Grant NA14NMF4410150) and CARICOOS (NOAA IOOS Grants NA11NOS0120035 & NA16NOS0120026).

Table of Contents

List of Tables.....	viii
List of Figures	ix
1. Introduction	1
1.1 Study area.....	2
1.2 Drifters	3
2. Objectives	6
2.1 Structure of the thesis	6
3. Drifter designs.....	8
3.1 In-house CODE-inspired drifter	8
3.2 Eco-friendly drifter.....	9
3.3 Post-processing.....	12
3.4 Velocity components.....	13
4. Surface circulation and lateral dispersion in the Mona Passage and off southwestern Puerto Rico as inferred from Lagrangian drifters.....	15
4.1 Introduction	15
4.1.1 Strategy of deployments	16
4.1.2 Spatial and temporal coverage of the data	19
4.2 Methods.....	23
4.2.1 Inter-comparison between drifter data and HF radar observations	23
4.2.2 Quantifying wind slippage.....	31
4.3 General circulation	33
4.3.1 Surface current properties in the Mona Passage.....	33
4.3.2 Mesoscale eddies	35
4.3.3 Tidal flows.....	36
4.3.4 Spectral analysis	36
4.4 Lagrangian dispersion	39
4.4.1 Absolute dispersion	40
4.4.2 Relative dispersion.....	41
5. Discussion and conclusions.....	51
References	56

List of Tables

Table 3.1 Summary of deployments conducted.....	12
Table 4.1a The IOA values are presented in two sub-tables: This first table shows the IOA values for the u (east-west) component comparisons.	29
Table 4.2b The IOA values are presented in two sub-tables: This second table shows the IOA values for the v (north-south) component comparisons.	30

List of Figures

Fig. 1.1 Bathymetry of the Mona Passage and off southwestern Puerto Rico. Colors represent depth in meters; intense reds indicate shallower areas. Source: NOAA.	2
Fig. 3.1 In-house CODE drifter design: (a) top view, (b) side view.....	9
Fig. 3.2 Design transition from in-house CODE drifter to the eco-friendly drifter.....	10
Fig. 3.3 Blueprint for eco drifter design.	11
Fig. 3.4 ECO drifter prototype after its first buoyancy trial run at CAOSE hydrostatic tank.	11
Fig. 3.5 Raw distance data and spike filtered distance data showing the values filtered out as empty black circles.	13
Fig. 3.6 Velocity components time series for the entire ECO drifter #1 track. Raw data shown in red, time filtered data from the spike filter shown in black, 10-min interpolated data shown in green, and 1-hr interpolated data shown in blue.	14
Fig. 4.1 Drifter launch patterns. [top] Nautical chart for the eastern side of the Mona Passage. Red markers indicate the positions of the six drifter triplets. Image source: NOAA. [bottom] In-set zoom of the drifter launch pattern for T1 (node to the south of LP). Inner Triangles: drifters at 100 meters apart. Outer Triangles: drifters at 2 km apart. The same launch pattern was used for T2 (node within the MP).	18
Fig. 4.2 Total time of active drifter trajectories in the water by drifter number. [top] Temporal coverage of PVC drifter data collected in 2015. [bottom] Temporal coverage of ECO drifter data collected in 2017.	19
Fig. 4.3 Drifter tracks from PVC drifters (top panel) and from ECO drifters (bottom panel). Drifter position color-coded to indicate days after deployment (left) and speed in m/s (right). ...	21

Fig. 4.4 Drifter tracks for PVC (2015) and ECO (2017) drifter deployments: farthest reach of individual drifters shown on the left; zoom-in to Mona Passage region shown on the right. Drifter position color-coded to indicate days after deployment.22

Fig. 4.5 CARICOOS HF radar network coverage. Snapshot from January 17, 2017 at 1:00 AM24

Fig. 4.6 CARICOOS HF radar network stations and their radial coverage during February 2015. The blue triangle indicates the FURA station in Rincón (left panel). The red triangle indicates the CDDO station in Cabo Rojo (right panel). Color bar indicates percent coverage.....25

Fig. 4.7 Comparison plots between the velocity time series derived from drifter PVC #7's trajectory and the velocity time series derived from HF Radar observations. Top left panel shows the comparison for the u (east-west) component and the lower left panel, for the v (north south) component. Drifter data is shown in magenta and HF Radar data in blue. Right side panel shows the drifter trajectory during the time window in which the drifter stayed within the HF Radar coverage. Drifter track is color coded to indicate days after deployment. Black triangles and black squares indicate first and last data points inside the HF Radar coverage, respectively.....26

Fig. 4.8 Comparison plots between velocity time series derived from drifter ECO #1's trajectory and the velocity time series derived from HF Radar observations. The same format as Fig. 4.7 was used.27

Fig. 4.9 Drifter speed (after removal of radar velocity) versus wind speed along radial direction shown in red. Least squared linear fit shown in magenta.32

Fig. 4.10 Progression of PVC drifters (#8, #9, and #10) as they were entrained in a mesoscale anticyclonic eddy. Color bar indicates sea surface height anomaly (above geoid) in meters.

Data courtesy of CoastWatch Caribb-NOAA AOML PhOD.....36

Fig. 4.11 [top panel] Track with number of days after deployment (left), and velocity magnitude (right) corresponding to each drifter position. In both plots, DR to the left, PR to the right.

[middle panel] U (left) and V (left) time series sectioned by region. The bounding boxes indicate the regions entered by the drifter: [1:2 days after deployment] = LP, [2:7] = MP, [7:20] = Northern DR [20:22] = Offshore DR [bottom panel] STFT results for the entire u (left) and v (right) time series using a 48-hr sample window with a 42-hr overlap.38

Fig. 4.12 Mean drift results for both nodes (triangles), T1 and T2, released as part of the ECO drifter deployment. [top] Zonal mean drift comparison (negative (-) indicates westward movement). [middle top] Meridional mean drift comparison. [middle bottom] Directions of the mean drifts of T1 positioned at their magnitude values. [bottom] Directions of the mean drifts of T2 positioned at their magnitude values. T1 results shown in blue; T2, in black.41

Fig. 4.13 Visual representation of the difference in spatial spreading between the two nodes deployed on April 2017.42

Fig. 4.14 Time evolution of the number of drifter pairs at given separation distances for the T1 (top), and T2 (bottom) releases (T1 = triangle released south of LP, T2 = triangle released within the MP). Increments at 50 m along the y-axis and 1-hr intervals along the x-axis. Data smoothed over 6-hr intervals.44

Fig. 4.15 Time series of cloud variance [top] along zonal direction, (D_x) and [middle] along meridional direction, (D_y), for T1 and T2 releases. [bottom] Time series of magnitude of

the cloud variance, D , for T1 and T2 releases. T1 shown in blue; T2. Particularly after day 7, spreading was significantly larger for LP (T1), than for MP (T2).45

Fig. 4.16 Mean square relative velocity as a function of pair separation. The solid lines indicate the best polynomial fit for the same colored data set. The blue and black symbols represent T1 and T2 results, respectively.....47

Fig. 4.17 Scale dependent pair separation rate, or relative dispersion rate, as a function of separation distance, r , for the T1 (in blue) and T2 (in black) deployments.48

Fig 4.18 Effective diffusivity as a function of separation distances. Fixed-scale average $K(r)$ vs separation distance (r) for the T1 (in blue) and T2 (in black) deployments.....50

Chapter 1

Introduction

The Mona Passage (MP), a vital shipping route between the Atlantic Ocean and the Panama Canal, connects waters (or water masses) from the Caribbean Sea and the Mid-Atlantic Ocean. The Mid-Atlantic being the source of saltier, more energetic (rougher), and deeper waters. Depths in the MP increase rapidly from 400 m at the top of the sill, which connects the northeast coast of the Dominican Republic (DR) to the southwest coast of Puerto Rico (PR), to below 4000 m. This drastic change in depth provokes sharp changes in the direction and strength of ocean currents. In addition, the waters in the MP are dominated by processes caused by the interaction between tidal and wind-driven currents, large-scale circulation, and mesoscale (spatial scales in the order of tens of kilometers) and submesoscale (spatial scales in the order of hundreds of meters) phenomena. This combination of factors contributes to the complexity of the flow along the eighty-mile wide passage. To better understand the general surface circulation modulated by these factors, several drifter deployments were conducted, intermittently, during a span of three years. For its upper ocean current-following abilities in the presence of wind and waves, an in-house drifter inspired by the Coastal Dynamics Experiment (CODE) drifter, introduced by Davis (1985), was implemented and, later, upgraded to an eco-friendly version to minimize the impact on ocean ecosystems.

1.1 Study area

The Mona Passage, located in the northwestern Caribbean within latitudes 17.8°N-18.6°N and longitudes 68.5°W-67.2°W, is known as one of the most treacherous routes in the Caribbean. Its chaotic and rapidly changing sea state often hinders the safe passage of commercial and passenger vessels within this area between PR and the DR. Due to the complexity of the bathymetry in the MP (see **Fig. 1.1**), sharp changes in the direction and strength of surface currents are very common in this region. The relatively shallow banks that characterize the MP, in many cases, induce strong surface currents that flow opposite to the winds and swells.

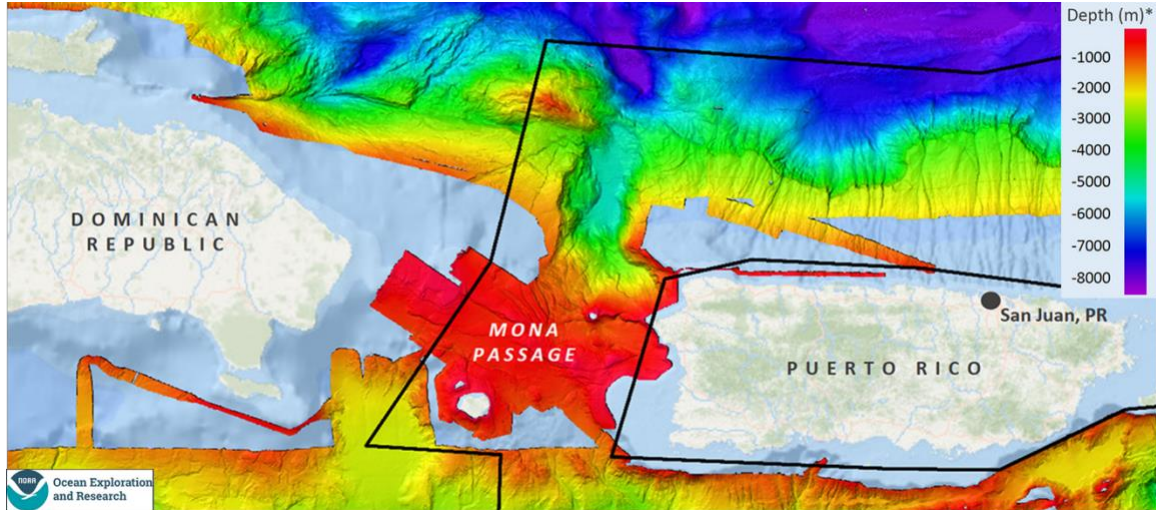


Fig. 1.1 Bathymetry of the Mona Passage and off southwestern Puerto Rico. Colors represent depth in meters; intense reds indicate shallower areas. Source: NOAA.

South Atlantic waters enter the Caribbean through the southern part of the Lesser Antilles Arc, while Gulf Stream waters, returning southwestward in the North Equatorial Current, enter the Caribbean through the passages north of Martinique (Johns et al. 2002). These waters cross the Caribbean from East to West and exit through the Yucatan Peninsula and the Florida Strait (Richardson 2005). After these waters enter the Gulf Stream, certain meanders are formed and

some of these waters return to the Caribbean through the Windward Passage and the MP as part of a vigorous exchange of waters between the Atlantic Ocean and the Caribbean Sea (Richardson 2005).

Some of the passages along the Antilles Island arc have been studied to a great extent, especially the passages in the Lower Antilles. The MP, forming part of the Greater Antilles passages, is not a part of that selected group. So far, the MP has been established as an inlet of Atlantic waters for the Caribbean Sea, carrying a net total of 4 Sv (Sverdrup) of these waters into the Caribbean (Johns et al. 2002), but there is little information describing how these waters behave as they cross the Passage. Studies regarding the Caribbean Sea (Johns et al. 2002; Richardson 2005) provide information concerning the MP, but these analyses are being conducted at such large scales that they do not allow for a detailed understanding of the circulation in the MP.

Currently, observational data from the MP consists of localized measurements from current profilers and wide-coverage measurements from high frequency radars and numerical models that are limited to certain temporal and spatial scales. These observations, which are more abundant to the eastern side of the Passage, are not enough to provide a description of the surface circulation patterns that dominate the whole region. Within this project's workframe, Lagrangian drifters were used to address these gaps in spatial data from surface currents in the MP. Two in-house surface drifter designs were developed in collaboration with the Caribbean Coastal Ocean Observing System (CARICOOS).

1.2 Drifters

Lagrangian drifters are surface drifting buoys, equipped with a GPS tracking device, that follow and help record the currents dominating the flow they are immersed in. These instruments

provide an approximation of the movement of a parcel of seawater confined to the ocean surface. As long as drifters can be assumed to act in true Lagrangian fashion, their trajectories can be used to understand possible transport pathways in the ocean. Factors that may cause a drifter to deviate from true Lagrangian trajectories include the effects of windage on the drifter structure. This factor will be addressed later in a separate section.

Drifter trajectories allow for the collection of position and velocity data at very high spatial and temporal scales. The contribution of drifters to oceanographic studies has included improvements in oil spill tracking, iceberg tracking and weather forecasting, and the calibration and validation of velocities from high frequency radars and altimeters (Lumpkin et al. 2016). Nowadays, the implementation of surface drifters for the study of upper ocean dynamics is a field of central importance to a wide range of natural and industrial applications (Salazar and Collins 2009).

The earliest record of Lagrangian measurements near the MP was published by Williams (1986). His paper recounts the trajectory of a single drifter drogued at 15 meters that was deployed off the north coast of PR. The drifter entered the MP and spent two months in the Caribbean Sea. In his article, Williams (1986) states that “the drifter’s small net movement [while it was to the north of PR] suggests little transport in [that] region and a long residence time for tracers.” The opposite is true for the MP; the drifter crossed the Passage “from 19°N in the North Atlantic to 17°N in the Caribbean in less than a week and moved at a mean speed of 38 cm/s, with the maximum speed over 60 cm/s” (Williams 1986). There were loops of different sizes present in the drifter track after the drifter left the MP, which suggest that the drifter was trapped in a cyclonic eddy. This is an occurrence that is not uncommon in the region, as will be shown later on by some of the data discussed in the present work. Lagrangian drifters have also been used to understand

the large-scale structure of the Caribbean Current, which flows westward through the southern part of the Caribbean. Richardson (2005) used satellite-tracked surface drifter trajectories to identify discrete cyclones and anticyclones that modulate the background flow of the Caribbean Current.

In recent years, many publications have focused on the oceanic flow properties that can be observed with drifters. These properties include single and two-particle dispersion in the upper ocean, a critical process that cannot be adequately observed with any other instrument. Two-particle dispersion has been an active research area since Richardson (1926) published his seminal paper about atmospheric diffusion (Salazar and Collins 2009).

Dispersion rates are important in a wide variety of applied problems that address questions regarding where water masses come from, where they go, and how fast they spread. It is defined as the rate at which a particle separates from its initial position or from another particle. The dispersion rates derived from drifter trajectories can shed light into the intricacies that dominate the dynamics of a specific region. For the case of strong and shifting currents in the MP, these dispersion rates can help reduce search areas in search and rescue missions, facilitate the quantification of connectivity between Marine Protected Areas (MPAs), and assist in the mitigation of possible oil spills.

Chapter 2

Objectives

The main objective of the present study is to understand the temporal and spatial scales of motion that play a significant role in the surface circulation of the Mona Passage and the waters to the southwest of Puerto Rico. The specific objectives of this study are:

- (1) Design, develop, and implement an eco-friendly drifter
- (2) Provide a qualitative description of the surface circulation patterns observed within the Mona Passage and the region off southwestern Puerto Rico
- (3) Quantify lateral dispersion processes for the Mona Passage and the region off southwestern Puerto Rico

The meeting of these objectives will result in a better understanding of the dispersion dynamics of particles, inferred from drifter trajectories, in the MP and to the southwest of Puerto Rico.

2.1 Structure of the thesis

The goal of this thesis is to increase our understanding of surface circulation and lateral dispersion in the Mona Passage and to the southwest of Puerto Rico. Chapter 3 includes an overview of the development of in-house drifter designs and an assessment of the post-processing required to identify and correct any inconsistencies in the drifter data, such as outliers and data gaps. Chapter 4 includes (1) a detailed description of the drifter data set, (2) the methods implemented to reinforce the validity of the drifter observations, (3) a depiction of the surface circulation patterns detected from drifter trajectories, and (4) an analysis of lateral drifter

dispersion. A numbered section was assigned to each item, respectively. The material contained in Chapter #4 was submitted as a separate article to a peer-reviewed scientific journal.

Chapter 3

Drifter designs

Current following drifters can describe the spatial structure of circulation at multiple scales and can be implemented in order to discover possible effects of topographic or bathymetric features (Davis, 1985). The following drifter designs are both considered low-cost, <\$500 for each (including the GPS tracker) and were both equipped with SPOT Trace® GPS tracking devices.

3.1 In-house CODE-inspired drifter

Inexpensive GPS-tracked drifters were built following the design of the Coastal Ocean Dynamics Experiment (CODE) drifter introduced by Russ E. Davis in 1985. The CODE design is well-known for its upper ocean current-following abilities in the presence of wind and waves. As shown in **Fig. 3.1**, the drifter design consists of four submerged sails, each measuring ~1 meter deep by ~0.5 meter wide, and a central mast with a GPS transmitter on top. These drifters were built in-house in the Center for Applied Ocean Sciences and Engineering (CAOSE) at the University of Puerto Rico at Mayagüez (UPRM). The materials needed to build these drifters were PVC (PolyVinyl Chloride) tubes with 3 inches in diameter for the central mast, PVC tubes with 1-1/2 inches in diameter for the framework that supports the vanes, vinyl fabric for the vanes, plastic tight wraps, a GPS transmitter, and a medium-size waterproof case.



Fig. 3.1 In-house CODE drifter design: (a) top view, (b) side view.

The first deployments contributed a total of 530 days of drifter data, which consists of more than 8,000 data points collected at a half an hour interval within an 8-month period, from February to September 2015.

3.2 Eco-friendly drifter

An eco-drifter can provide the observations that warranted its deployment without contributing to the amount of plastic waste in the ocean. Limiting the carbon footprint of oceanographic instruments, such as drifters, is a great advantage when large amounts of data are required to cover an area of interest (Poje et al. 2014). This is why an ecologically conscious design for a surface drifter was developed, assembled and tested in open water for the second round of deployments.

The design, as shown in **Fig. 3.3**, consists of two virola wooden panels cut halfway down the middle that interlock with one another to assemble a cross¹. Pine wood rods were used as

¹ Two other eco-friendly drifter designs were assembled and tested in open water: one made out of bamboo and another with a pine wood frame. These designs did not meet the expected requirements of lasting neutral buoyancy and had to be revised.

screws, and both wooden panels were coated with an eco-friendly wood sealant to prevent water absorption. The design and prime material adjustments minimized the need for foam floats, plastic tight wraps, and stainless-steel screws. The electronic component of the drifter and its waterproof casing were not altered. Since these drifters have a less negative impact on the environment, a major eco-friendly drifter deployment was conducted. A total of 18 eco-friendly drifters were deployed in two separate arrangements within the high frequency radar coverage of the Mona Passage. The deployment took place in late April 2017, and the drifters were released within a small time-window, just a couple of hours apart, so it could be considered a simultaneous deployment.

In the case of the Mona Passage, deploying several drifters simultaneously, which had not been done before, provided observations that describe the local surface circulation from a whole new perspective.

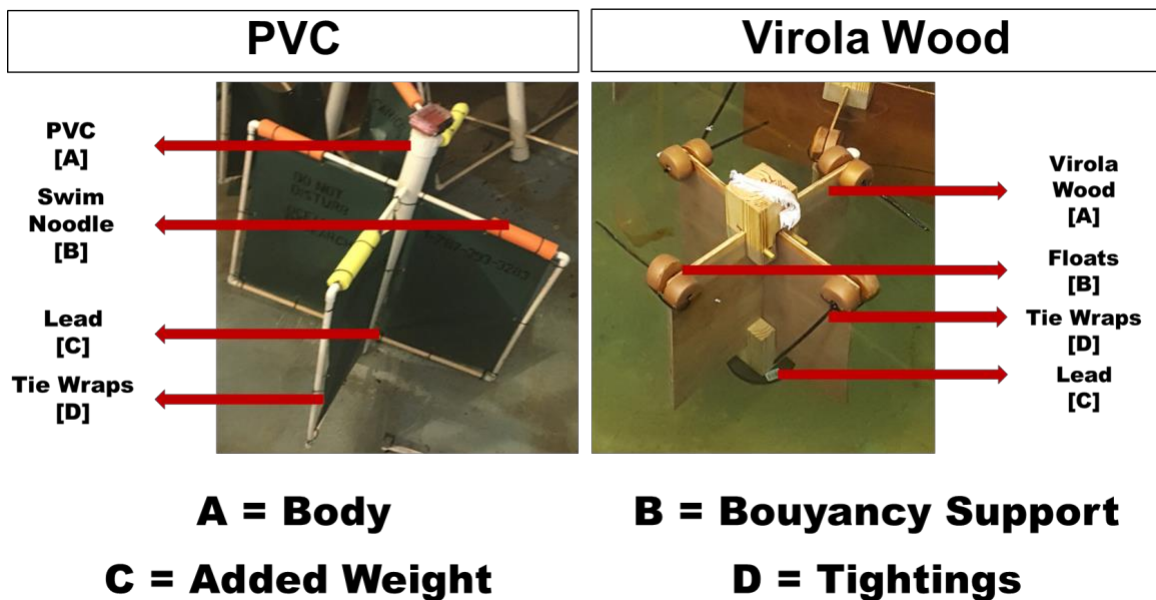


Fig. 3.2 Design transition from in-house CODE drifter to the eco-friendly drifter.

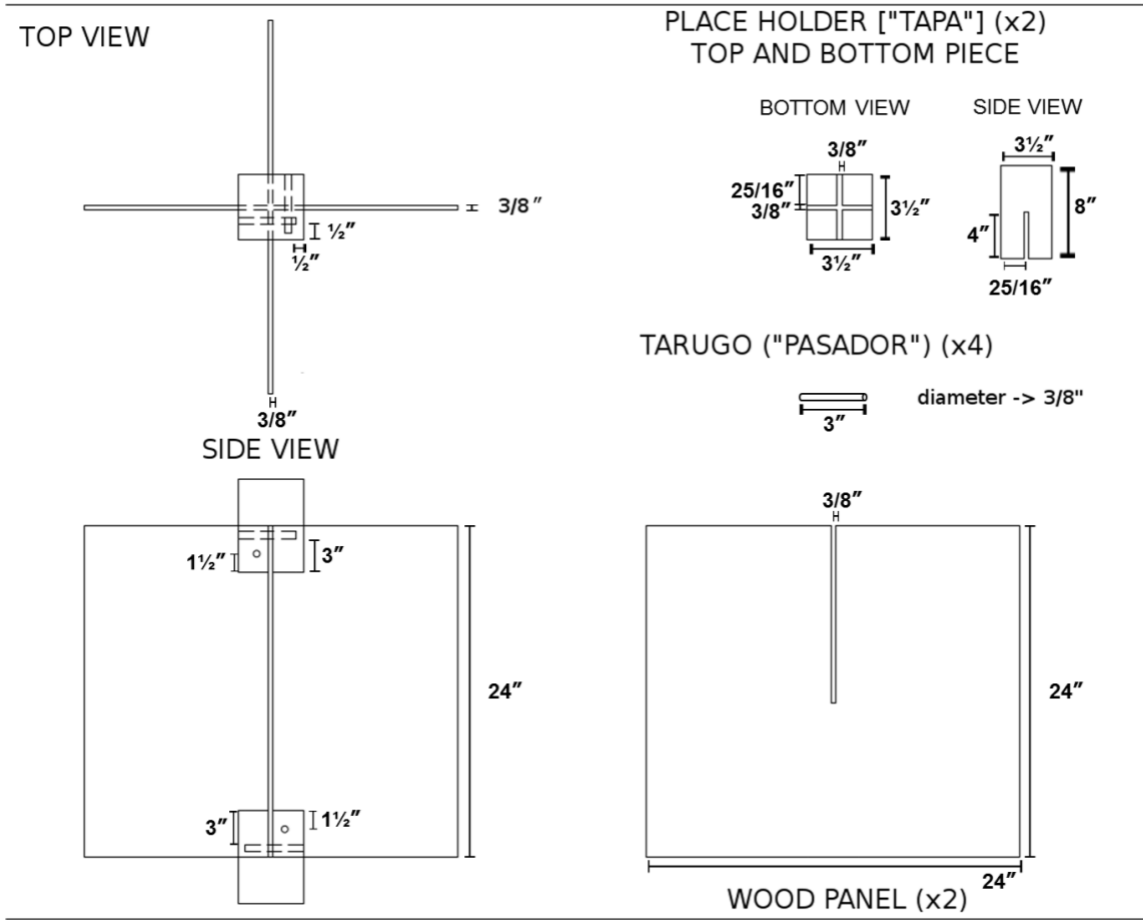


Fig. 3.3 Blueprint for eco drifter design.



Fig. 3.4 ECO drifter prototype after its first buoyancy trial run at CAOSE hydrostatic tank.

Table 3.1 Summary of deployments conducted.

Date	Identifier (# of drifters)	Buoy days [Data]	Design
Feb-Jun 2015	MPAs (14)	461	PVC
Aug-Oct 2015	MPAs (3)	69	PVC
Apr-May 2017	Mini Eco (20)	330	ECO

3.3 Post-processing

The initial drifter data set consisted of a raw time series for the drifter positions. The positions were represented by the latitudinal and longitudinal coordinates of the drifter. The GPS tracker instrument was set to take a location measurement every 10 minutes for the ECO drifters and every 30 minutes for the PVC drifters. The raw data obtained had certain gaps that needed to be filled in order to keep the same data resolution along the entire drifter track, and some data points needed to be removed because they were the result of an error in the GPS tracker measurement. Spurious position data points, which resulted in unrealistic velocity estimates, were removed using a time filter and a spike filter.

The time filter consisted of calculating the number of minutes between data points, identifying the drifter positions that correspond to less than 5 minutes, and creating a new time series that did not include those positions. The spike filter consisted of evaluating whether or not the distance between consecutive data points was above the 75th percentile plus 1.5 times the Interquartile Range (IQR) or below the 25th percentile minus 1.5 times the IQR. The 25th, 50th, and 75th percentiles, and the IQR were calculated using the entire time series for each drifter. If a distance complied with either one of the previously stated conditions, that distance was considered

a spike in the data and the corresponding data point removed from the time series. **Fig. 3.5** shows the distance time series before it was filtered (black circles), and after the spike filter was applied (black circles filled red).

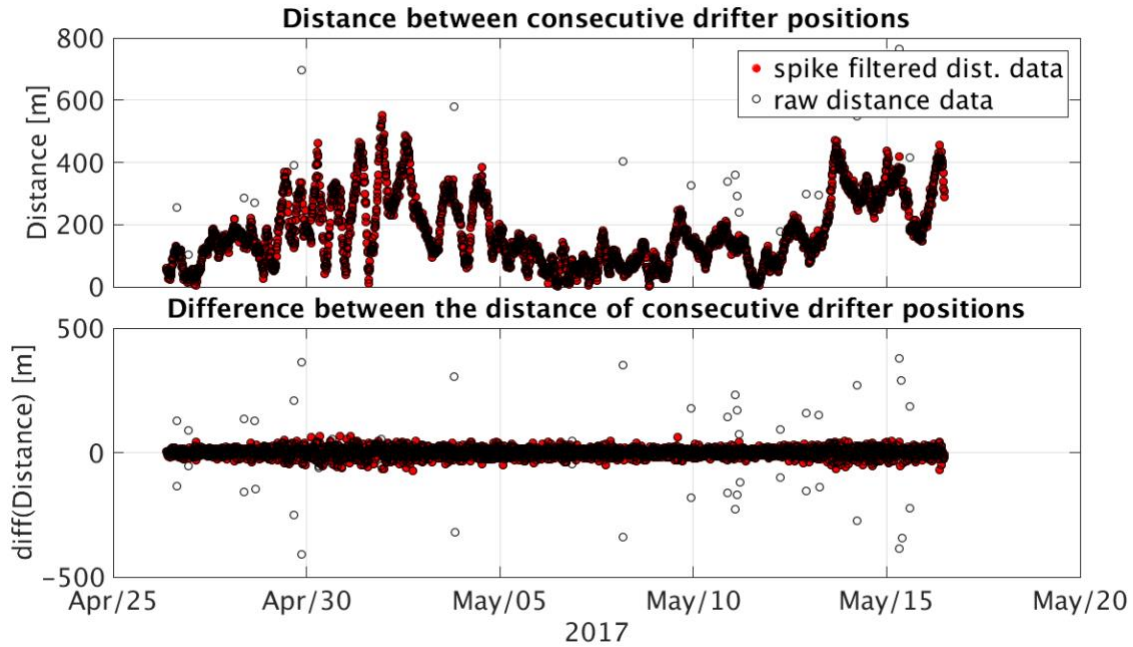


Fig. 3.5 Raw distance data and spike filtered distance data showing the values filtered out as empty black circles.

3.4 Velocity components

The u (east-west) and v (north-south) components of the drifters' velocities were derived using the time and spike filtered position time series. To maintain the same temporal resolution throughout the drifter data set, u and v components were interpolated to 1-hr and 10-min intervals using a trend following spline interpolation. The spectral analysis of the drifter velocity time series, which will be discussed in a separate section, was conducted using the 10-min interpolated data. For the dispersion analysis, the comparison between drifter data and HF radar observations, and the windage quantification, the 1-hr interpolated drifter data was used instead.

As the resulting velocity time series were plotted, oscillations with a greater amplitude than during the rest of the drifter track could be easily identified. The time at which those oscillations with greater amplitudes occurred was referenced to the drifter's location at that time, and it turns out that those time periods correspond to the time that the drifter spent within the Mona Passage region. **Fig. 3.6** shows an example from ECO drifter #1. There are oscillations with a greater amplitude between April 28 and May 04. These time period corresponds to the week that the drifter spent within the Mona Passage region. See **Section 4.3.4** for a spectral analysis of the drifter oscillations during this time period.

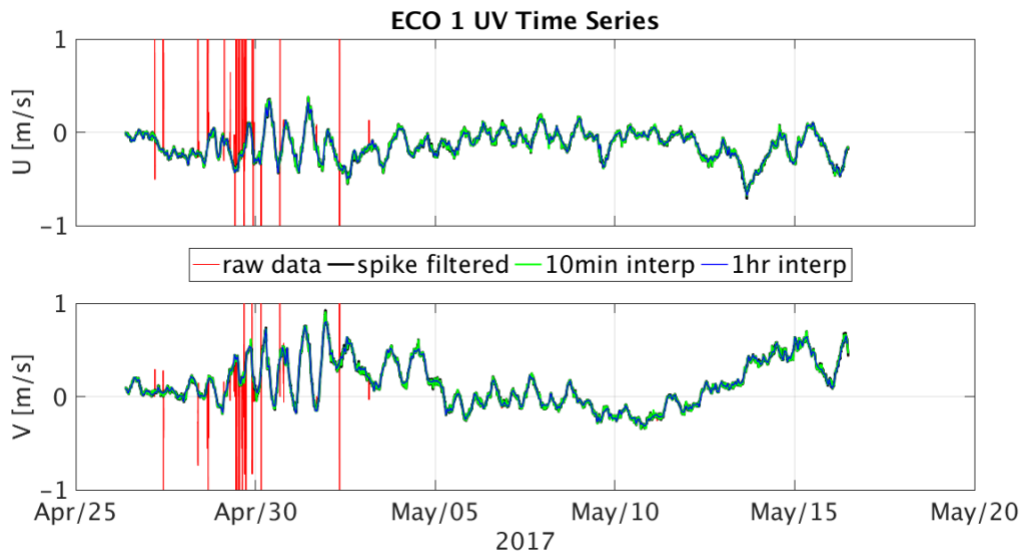


Fig. 3.6 Velocity components time series for the entire ECO drifter #1 track. Raw data shown in red, time filtered data from the spike filter shown in black, 10-min interpolated data shown in green, and 1-hr interpolated data shown in blue.

Chapter 4

Surface circulation and lateral dispersion in the Mona Passage and off southwestern Puerto Rico as inferred from Lagrangian drifters

The material in this chapter is an expanded version of the article “Surface circulation and lateral dispersion in the Mona Passage and off southwestern Puerto Rico as inferred from Lagrangian drifters” by Estefanía Quiñones-Meléndez and Miguel Canals, which was submitted for publication to a peer-reviewed journal.

This chapter will include a description of the Mona Passage, an assessment of the drifter data, an inter-comparison between surface current velocities from drifters and high-frequency radars, a qualitative description of the oceanographic phenomena that control surface currents in this region (i.e., mesoscale and submesoscale eddies, tidal forcing, etc.), and a statistical analysis of drifters’ trajectories from a Lagrangian perspective.

4.1 Introduction

The analysis presented in this work will focus on understanding the general circulation described by drifter trajectories and by the lateral dispersion measurements derived from those trajectories. The analysis of drifter dispersion rates will enable the improvement of hydrodynamic models currently being implemented for the US Caribbean. Hydrodynamic numerical models

currently implemented in PR (i.e., ROMS, AMSEAS) apply default coefficients that may not necessarily reflect the local dispersion processes of the area that is being modelled.

4.1.1 Strategy of deployments

The first drifter deployments took place in early 2015, from February to March, and continuous drifter data was collected until early May. Many of these deployments took place in the month of February, coinciding with spawning events within the MPAs off the west coast of PR. The second round of drifter deployments was conducted in 2015 as well, but this time from April to August. These drifters were released in pairs and groups of three, but they were not organized with the purpose of measuring dispersion rates. These drifters had submerged vanes measuring ~1 m in depth, and their primary building material was PVC tubing. Drifters from these deployments will be referred to as “PVC” drifters.

Another drifter deployment was designed with a focus on measuring dispersion in the MP and off southwestern PR. On this occasion, a different drifter design was utilized in order to minimize the impact on ocean ecosystems. The new drifter measured three fifths ($3/5$) of the PVC drifter’s depth (height), which made for a more compact and mobile version of the PVC drifter. Drifters from these deployments will be referred to as “ECO” drifters.

The ECO drifter deployment was conducted on April 26th, 2017. A total of 18 ECO drifters were deployed following a similar arrangement strategy to the one proposed by Poje et al. (2014): drifters arranged in 2 nodes spaced at ~70 km with each node containing nine drifters arranged in triplets of nested equilateral triangles, with separations of 100 m between drifters within a triplet and of 2 km between triplets within a node, as shown in **Fig. 4.1**. These drifters were released in groups of three to enable the quantification of dispersion rates. Every node generated a total of 36

drifter pairs with initial separation distances ranging from 100 m to 2 km. The first node was located south of PR, with its center at latitude 17.788°N and longitude 67.032°W , to cover the demand of drifter data for the region off southwestern PR. To deploy these drifters, operations briefly moved to a small coastal town along the southern coast of PR known as La Parguera (LP). This first node will be addressed as T1 from now on. The second node was located within the MP, with its center at latitude 18.218°N and longitude 67.505°W and will be addressed as T2 from now on.

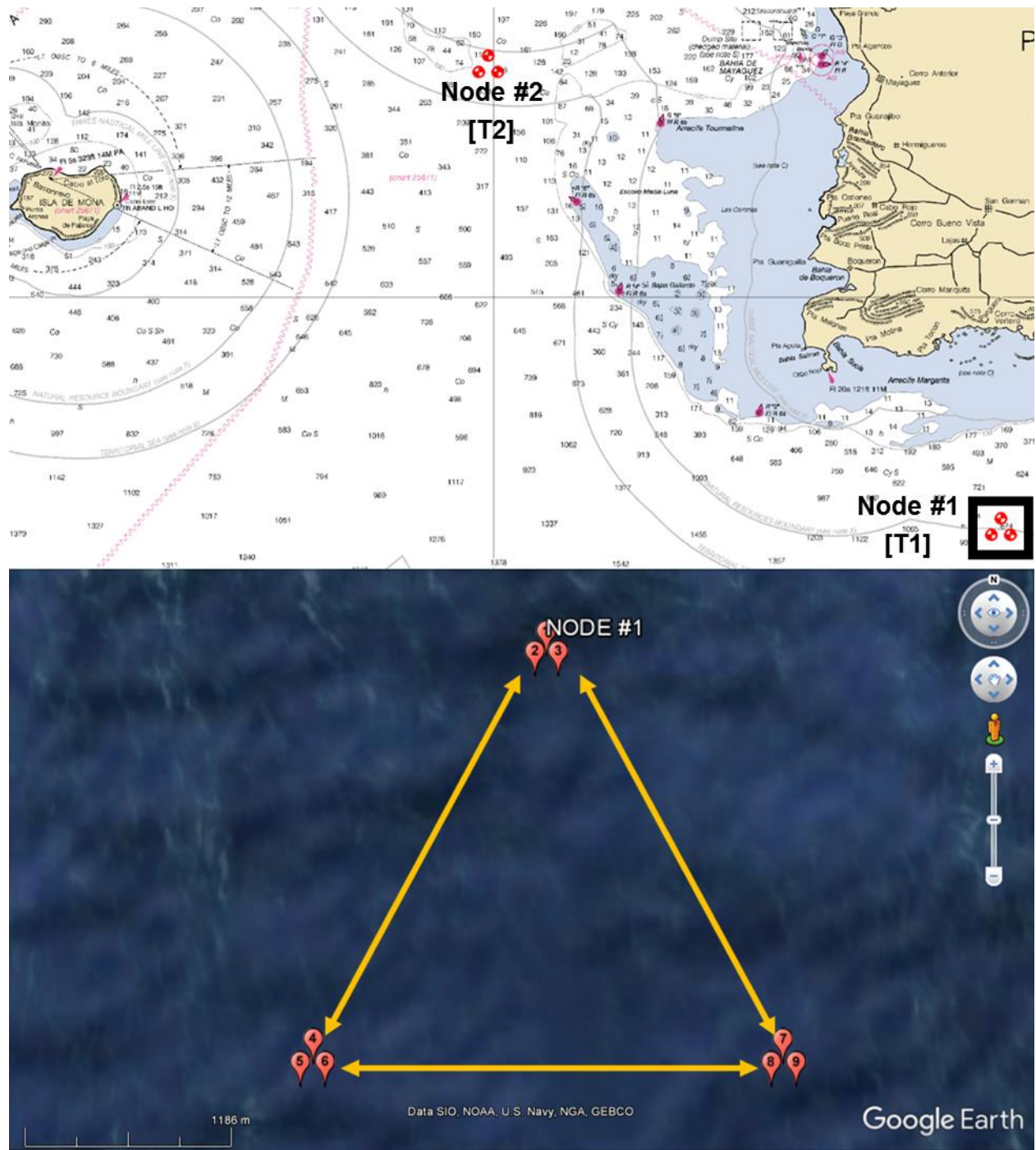


Fig. 4.1 Drifter launch patterns. [top] Nautical chart for the eastern side of the Mona Passage. Red markers indicate the positions of the six drifter triplets. Image source: NOAA. [bottom] In-set zoom of the drifter launch pattern for T1 (node to the south of LP). Inner Triangles: drifters at 100 meters apart. Outer Triangles: drifters at 2 km apart. The same launch pattern was used for T2 (node within the MP).

4.1.2 Spatial and temporal coverage of the data

The present study aims to understand the temporal and spatial scales of motion that play a significant role in the surface circulation of the MP and the waters to the southwest of PR.

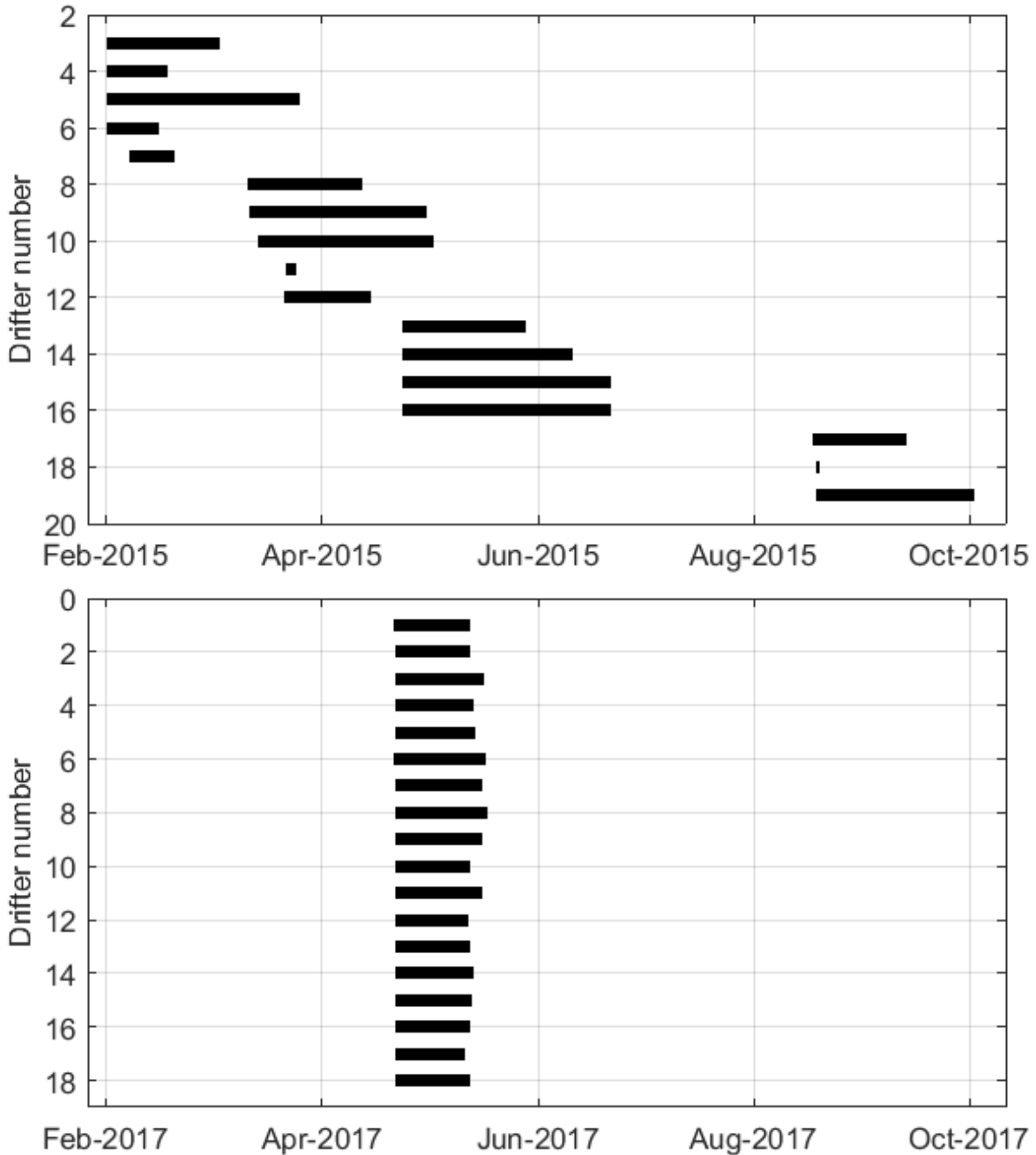


Fig. 4.2 Total time of active drifter trajectories in the water by drifter number. [top] Temporal coverage of PVC drifter data collected in 2015. [bottom] Temporal coverage of ECO drifter data collected in 2017.

On the top panel, **Fig. 4.2** shows the individual time coverage of the first 17 deployments made with PVC drifters (drifters #3 to #19). On the second panel, **Fig. 4.2** shows the individual time coverage of the 20 drifters that were deployed as part of the largest simultaneous deployment of drifters within the MP and the southwest of PR. This drifter deployment was carried out with ECO drifters, a drifter design focused on implementing eco-friendly materials in order to mitigate the plausible pollution of these instruments that are not retrieved after their deployments.

On the top left panel, **Fig. 4.3** shows the trajectories traced by the fourteen drifters deployed from February to April 2015. These image shows how much of the MP was covered by the drifters, and the number of days each drifter stayed within the MP. The fourteen drifters were deployed at different times; that is why some moved southward, while others moved northwestward. As it turns out, different oceanographic conditions dominated the MP region throughout the 20-day period the drifters were inside the passage (more details in **Section 4.3**).

The dates in which the drifters were deployed, and the amount of time spent in the water has been stated because some seasonal variability could be possible in the results and it was a notion present during the analysis. Therefore, tracks from different deployments were carefully included in the same graphic.

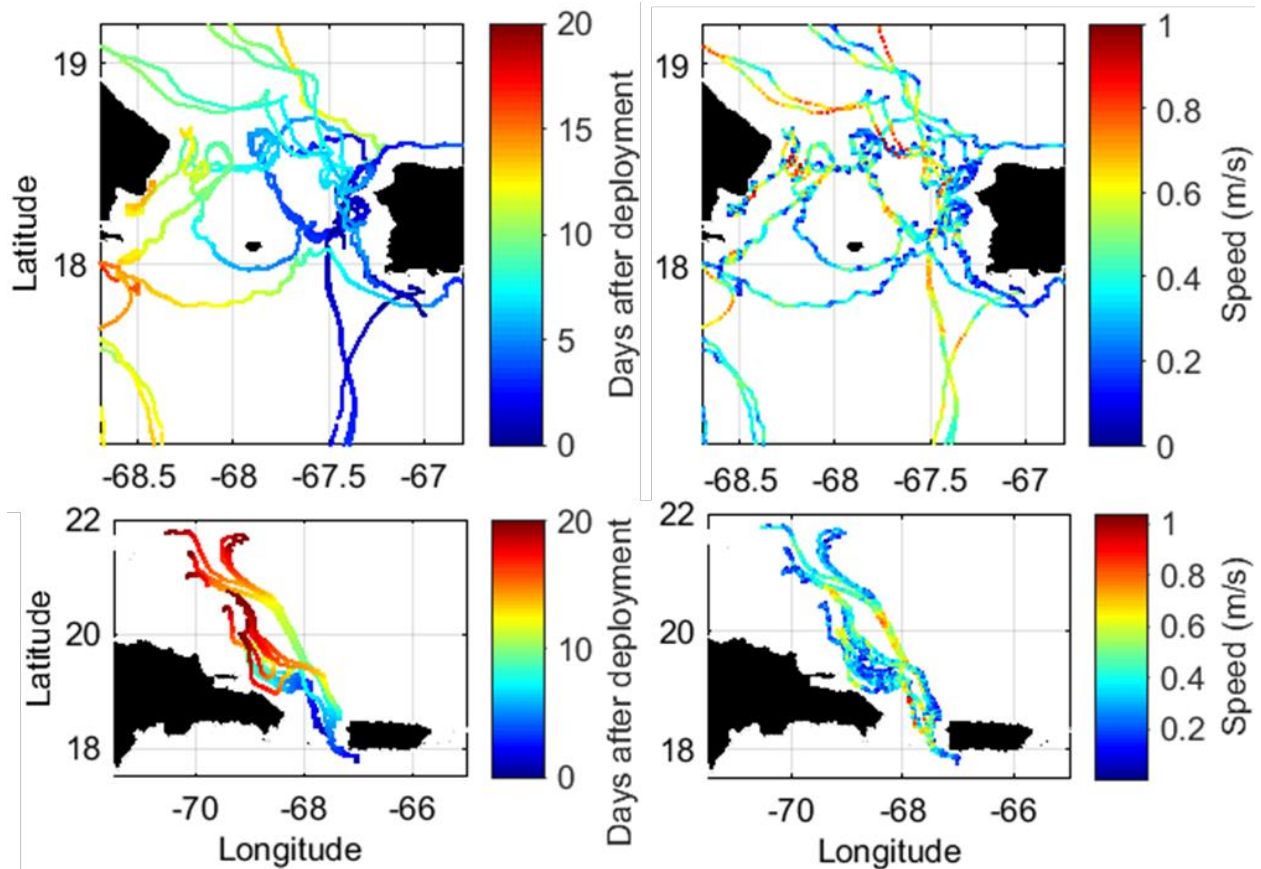


Fig. 4.3 Drifter tracks from PVC drifters (top panel) and from ECO drifters (bottom panel). Drifter position color-coded to indicate days after deployment (left) and speed in m/s (right).

Fig. 4.3 also shows the trajectories traced by ECO drifters and the resulting velocity magnitude for each drifter position. When comparing these second images to the ones from the 2015 deployment, the most obvious difference is that all drifters are moving in the same direction: northwest. Drifter coverage is significantly reduced for the 2017 deployment, but this is expected since these drifters were released at the same time, all subject to the same oceanographic conditions.

Fig. 4.4 shows all drifter trajectories, color coded by days after deployment, showing that ECO drifters were able to reach same distances as PVC drifters in a shorter amount of time. The

difference between the amount of time it took the PVC and ECO drifters to reach this region could be the result of several factors such as a stronger mean flow and/or different oceanographic conditions. Both sets of drifter data (PVC and ECO) were compared to surface current velocity observations from high frequency radars in **Section 4.2.1**. In that section, we show that the difference in days after deployment that it took drifters to reach the Turks and Caicos region is not likely a result of the design modifications implemented in order to create the ECO drifter.

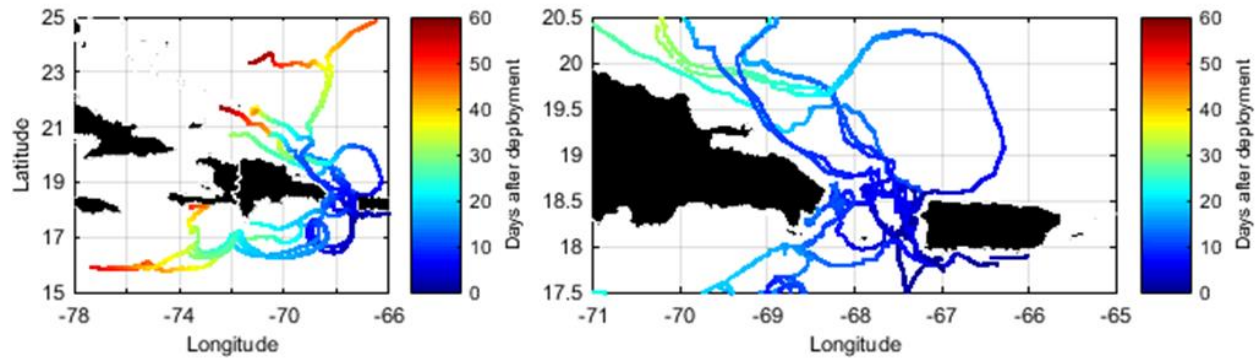


Fig. 4.4 Drifter tracks for PVC (2015) and ECO (2017) drifter deployments: farthest reach of individual drifters shown on the left; zoom-in to Mona Passage region shown on the right. Drifter position color-coded to indicate days after deployment.

Section 4.2 presents the methods implemented in order to reinforce the validity of the obtained drifter observations: a comparison between surface current velocities from drifters and high frequency radars, and wind drift (or slippage) quantification. The rest of this chapter is divided into two sections: **Section 4.3** includes a description of the surface circulation patterns of the MP detected from drifter trajectories, and **Section 4.4** presents the analysis of lateral drifter dispersion in the region of the MP and to the southwest of PR.

4.2 Methods

4.2.1 Inter-comparison between drifter data and HF radar observations

High frequency (HF) radar stations have been recently installed by CARICOOS along PR's coastline in order to obtain real time observations of surface currents (see **Fig. 4.5**). Two stations cover the eastern side of the MP (FURA and CDDO) and three stations cover waters to the southwest, south and southeast of PR (FARO, PYFC and MABO, respectively). Combined, these stations provide hourly observations of surface current speed and direction that can be compared with the velocity observations derived from drifter displacements. An inter-comparison between drifter movements and HF radar vector fields was implemented to demonstrate that both drifter designs correctly follow the surface current patterns observed by CARICOOS HF radar network.

HF radar technology uses an array of antennas to estimate the surface velocity of ocean currents by quantifying the Doppler shift caused by ocean currents on surface waves. Each antenna provides velocity measurements for fixed locations in space along specific radial directions. Radials can only provide measurements of the component of the velocity that is along its direction or that opposes that direction by a 180-degree angle. But if two or more radials from nearby antennas coincide at an angle that is far from parallel, the radial measurements from both antennas can generate a total velocity vector, which is a measurement of the surface current velocity in terms of u and v components; in other words, independent of the reference frame of a single radial velocity estimate. HF radials were used for the inter-comparison between HF radar and drifter data since radials can provide a much finer spatial resolution than HF-derived total velocities. For comparison, drifter velocities were projected onto the HFR-derived radial velocity vectors to obtain drifter-derived radial velocities at the location of the HFR measurements.

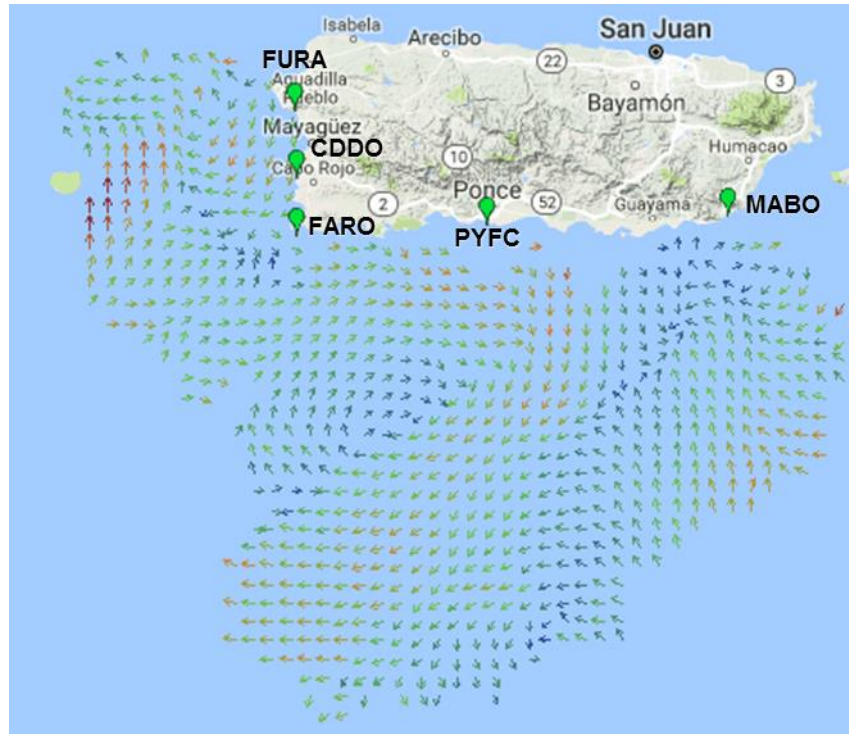


Fig. 4.5 CARICOOS HF radar network coverage. Snapshot from January 17, 2017 at 1:00 AM (Source: www.CARICOOS.org/hf-radar).

CARICOOS HF radars were fully operational during the drifter deployment periods and provided real-time measurements of the surface current conditions for the eastern part of the MP and the waters to the southwest of PR. **Fig. 4.6** shows the percent radial coverage, corresponding to February 2015, for each of the two HF radar stations facing the MP.

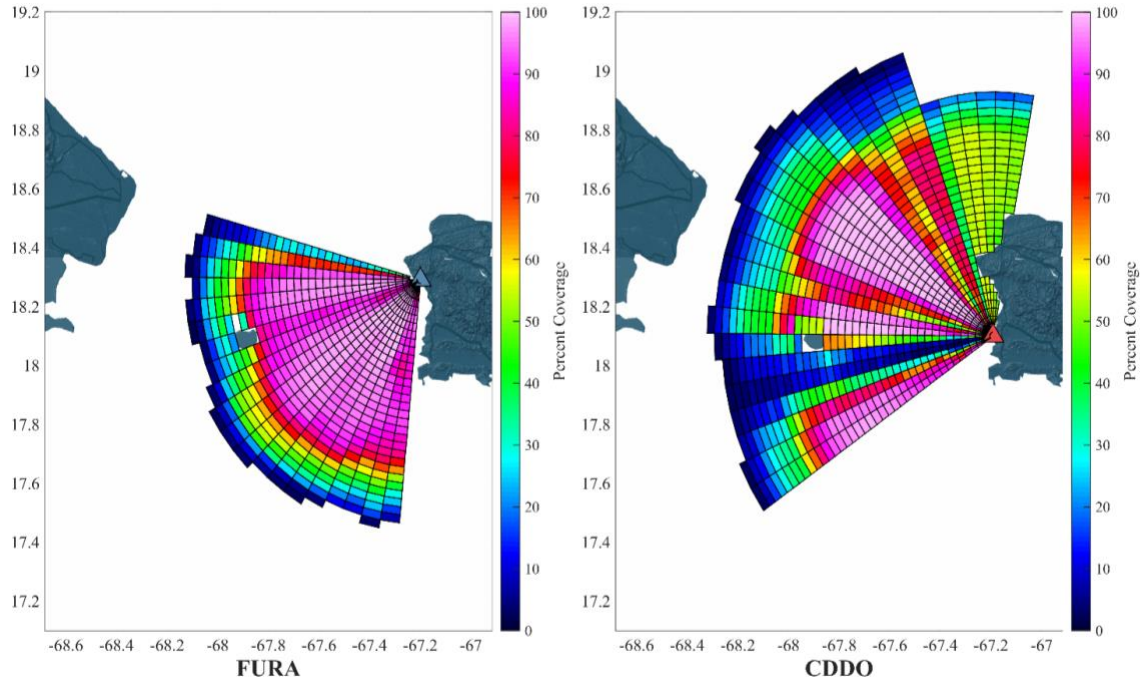


Fig. 4.6 CARICOOS HF radar network stations and their radial coverage during February 2015. The blue triangle indicates the FURA station in Rincón (left panel). The red triangle indicates the CDDO station in Cabo Rojo (right panel). Color bar indicates percent coverage.

Two comparisons between the drifters and the HF radar will be presented and discussed in this section: one time series from each drifter deployment (PVC and ECO deployments). The first will be the time series from drifter PVC #7 from the mid-February 2015 deployment. The second time series will be from drifter ECO #1 from the April 2017 deployment. The comparison plots for these drifter-derived velocity time series can be found in **Fig. 4.7** and **Fig. 4.8**, respectively. An index of agreement (IOA) value corresponding to each comparison was calculated to detect differences between both velocity measurements using the following equation: $IOA = 1 -$

$$\frac{\langle (x_c - x_m)^2 \rangle}{\langle (|x_c - x_c| + |x_m - x_m|)^2 \rangle}$$

where x_c represents the drifter data, x_m represents the corresponding HF

Radar data and the $\langle \ \rangle$ operator indicates an average. This metric must not be used to determine an error since differences between the two data sets are to be expected given the differences in

temporal and spatial resolution from both sets of measurements and the distinct methods involved to obtain those measurements. Through this comparison, we are interested in determining whether the large-scale drifter movements compare favorably with the HF radar vector fields.

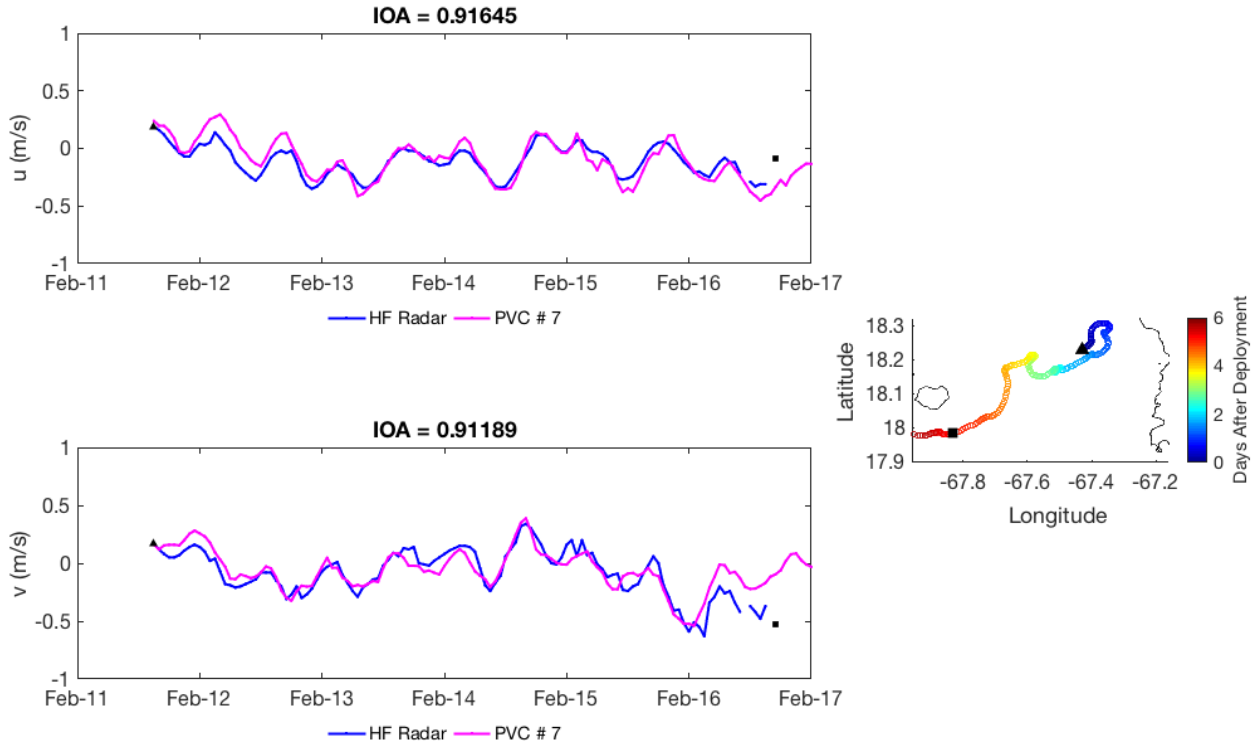


Fig. 4.7 Comparison plots between the velocity time series derived from drifter PVC #7's trajectory and the velocity time series derived from HF Radar observations. Top left panel shows the comparison for the u (east-west) component and the lower left panel, for the v (north south) component. Drifter data is shown in magenta and HF Radar data in blue. Right side panel shows the drifter trajectory during the time window in which the drifter stayed within the HF Radar coverage. Drifter track is color coded to indicate days after deployment. Black triangles and black squares indicate first and last data points inside the HF Radar coverage, respectively.

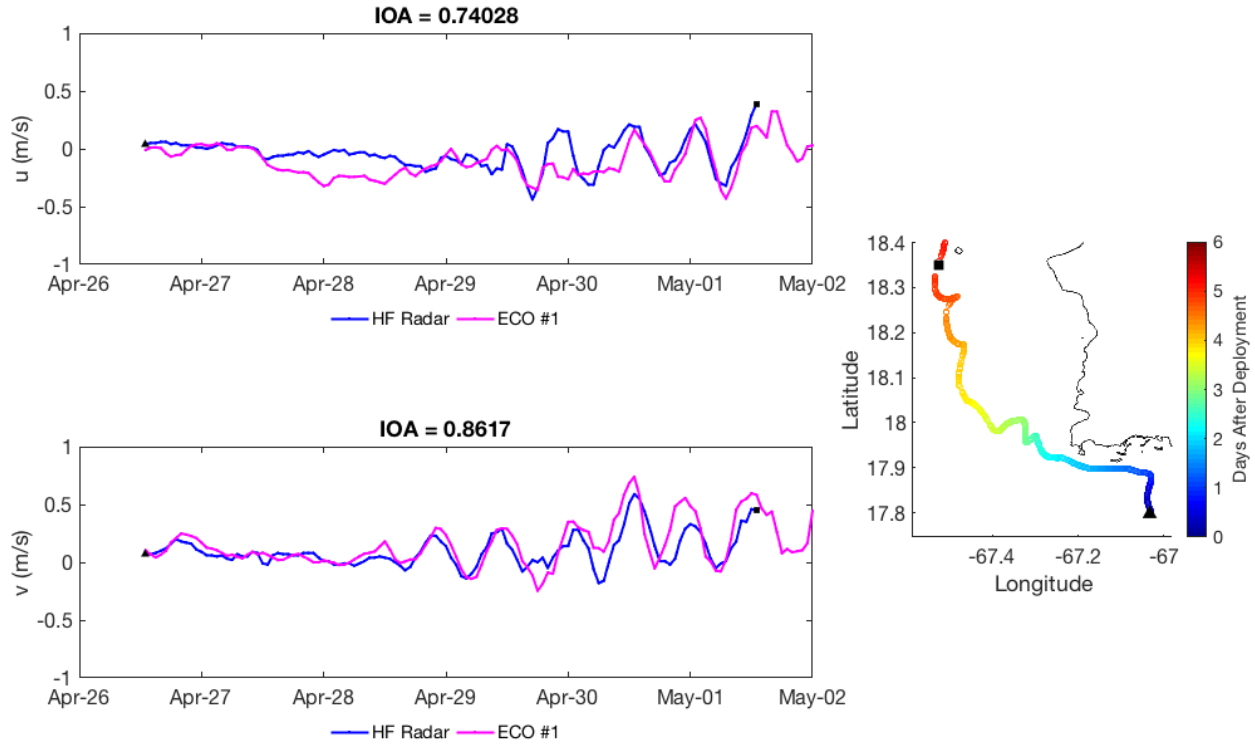


Fig. 4.8 Comparison plots between velocity time series derived from drifter ECO #1's trajectory and the velocity time series derived from HF Radar observations. The same format from **Fig. 4.7** was used.

Each comparison plot also contains the drifter track or trajectory as a reference, and is color coded to indicate the number of days after its deployment. Drifter tracks generally lasted between one and two months, but the tracks and the time series in the comparison plots only show data for the days that the drifters were within the footprint of the HF radar coverage. In every plot, the velocity component derived from the HF Radar is shown in blue and the component derived from the drifter tracks is shown in magenta. The drifter observations coincide quite well with the HF Radar observations. Both time series follow a similar trend, and the drifter observations peak at the same time as the HF Radar observations. The most notable difference between both sets of observations is the amplitude of these peaks, although this is to be expected since the HF Radar operates on a coarser grid and uses spatial averaging which introduces some spatial smoothing to the velocity fields.

While only the time series comparison for two drifters has been shown here, results were very similar for all drifter trajectories, as shown in **Table 4.1**. The IOA values for every drifter deployment are within the range of 0.6727 and 0.9443. Since a value of 1 indicates a perfect match, and 0 indicates no agreement at all, it holds that the large-scale drifter movements compare favorably with the HF radar vector fields. The lowest IOA values reflect some discrepancies between the two sets of observations. A possible source for these discrepancies could be the wind effects on the drifters (see **Section 4.2.2**). Nevertheless, the figures and analysis shown in the previous pages demonstrate that both surface drifter designs implemented in this project appropriately follow the surface current fields in the MP.

Table 4.1a The IOA values are presented in two sub-tables: This first table shows the IOA values for the u (east-west) component comparisons.

DESIGN	DRIFTER NUMBER	IOA	Drifter Arrangement	Average IOA	DESIGN	DRIFTER NUMBER	IOA	Coupled Deployment	Average IOA	
ECO	#1	0.7403	T1	0.7741	PVC	#3	0.8697	FEB 2015	0.8281	
	#2	0.7571				#4	0.8166			
	#3	0.7374				#5	0.7594			
	#4	0.8054				#6	0.7784			
	#5	0.7732				#7	0.9165			
	#6	0.7926				#8	0.9304			
	#7	0.8007				#9	0.9351			
	#8	0.7765				#10	Out of Coverage			
	#9	0.7839	#11	Out of Coverage		MAR 2015	0.8927			
	#10	0.8350	#12	0.8125						
	#11	0.8475	T2	0.8534		#13	0.9330	APR 2015	0.8925	
	#12	0.8466				#14	0.8736			
	#13	0.8669				#15	0.9335			
	#14	0.8634				#16	0.8297			
	#15	0.8807				#17	0.6727			
	#16	0.8494				#18	0.6930	AUG 2015		0.7193
	#17	0.8570				#19	0.7921			
	#18	0.8343								

Table 4.2b The IOA values are presented in two sub-tables: This second table shows the IOA values for the v (north-south) component comparisons.

DESIGN	DRIFTER NUMBER	IOA	Drifter Arrangement	Average IOA	DESIGN	DRIFTER NUMBER	IOA	Coupled Deployment	Average IOA	
ECO	#1	0.8617	T1	0.8640	PVC	#3	0.3582	FEB 2015	0.7074	
	#2	0.8663				#4	0.7637			
	#3	0.8682				#5	0.7420			
	#4	0.8699				#6	0.7610			
	#5	0.8811				#7	0.9119			
	#6	0.8107				#8	0.8346	MAR 2015		0.8412
	#7	0.8667				#9	0.8362			
	#8	0.8722				#10	Out of Coverage			
	#9	0.8792				#11	Out of Coverage			
	#10	0.6485	T2	0.6927		#12	0.8527	APR 2015	0.9294	
	#11	0.6883				#13	0.9443			
	#12	0.6863				#14	0.9187			
	#13	0.6053				#15	0.9433			
	#14	0.5726				#16	0.9113			
	#15	0.5939				#17	0.8450	AUG 2015		0.8293
	#16	0.8224				#18	0.7180			
	#17	0.7907				#19	0.9250			
	#18	0.8260								

4.2.2 Quantifying wind slippage

The wind field over PR is dominated by the trade winds, but the wind forcing over the MP undergoes strong variability at hourly and daily time scales. The central chain of mountains running along the island interacts with the trade winds through flow-topography interaction. This interaction causes convection and an island wake wind effect over the MP that can generate thunderstorms and heavy rain showers. As a result, the wind field over the MP is characterized by the generation of storms that can quickly move over the region.

CODE-style drifters typically experience a wind slip on the order of 3% of the wind velocity (Poulain 2001), which causes the drifters to deviate from true Lagrangian trajectories. In comparison, for drifters drogued at 15 m, the slippage on the drifters since the transfer of momentum to the surface buoy from waves and winds is minimized through their design and is estimated to be 0.1% of the wind speed (Niiler et al. 1995). This error is about as large as that associated with the satellite positioning. The CODE drifters were also designed to reduce wind slippage, but the effect may still persist under high wind and sea conditions.

High frequency (HF) radars were instrumental in quantifying the wind slippage affecting the eco-friendly surface drifter design and comparing the wind slippage experienced by both drifters. We must keep in mind that wind-driven ocean circulation can strongly influence current systems in the upper few hundred meters of the ocean, while the drifters only measure the first meter of the water column.

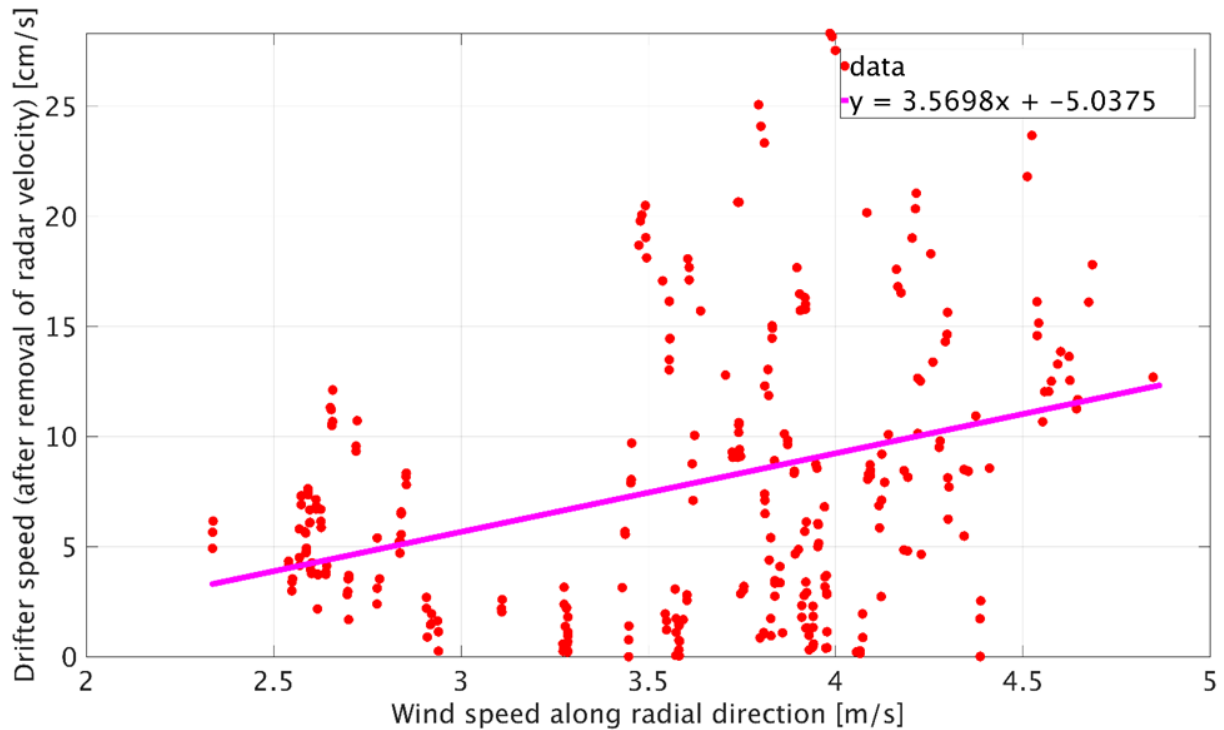


Fig. 4.9 Drifter speed (after removal of radar velocity) versus wind speed along radial direction shown in red. Least squared linear fit shown in magenta.

Using the nearest radials to drifter positions, adjusted drifter speeds were obtained by removing the HFR-derived surface current velocities from the original drifter velocities projected onto the radial vectors. **Fig. 4.9** shows the adjusted drifter speeds plotted against wind speeds obtained from the CARICOOS 1-km resolution Weather Research Forecasting (WRF) operational model (Aponte et al. 2015). The model wind velocities were also projected onto the same radial direction as the original drifter velocities. Reproducing the analysis published by Poulain et al. (2009), the figure also shows a linear fit which purpose is to provide a rough estimate of the relationship between incident wind speed and drifter speed. While there is significant variability in the wind-slip estimates, the least-squared linear fit suggests a wind-induced drift of approximately 3.5% of the modelled wind speed. This rough estimate fits within the parameters described by Poulain et al. (2009) for CODE-style drifter designs. The drifter speeds used to

generate **Fig. 4.9** were from ECO #1. These results, combined with the favorable comparison between the drifter and HFR-derived velocities, suggests that the drifters offer a satisfactory estimate of upper-ocean surface currents, at least as good as what would be expected using the widely used CODE design.

4.3 General circulation

This section will include a qualitative description of the oceanographic phenomena that control surface currents in the MP region. In light of the drifter movements observed, a detailed description of the varying surface circulation patterns of the MP is presented here. As previously mentioned, the waters in the MP are dominated by processes caused by the interaction between tidal currents, large-scale circulation and mesoscale phenomena. The influence of these factors on drifter movements, and consequently on the surface current patterns of the MP, will be presented in this section.

4.3.1 Surface current properties in the Mona Passage

The complexity of the regional bathymetry plays a significant role in the general shape of the surface circulation pattern of the MP. As described by Baums et al. (2006), the drastic change in depth that characterizes the MP's sill is conducive to the formation of long-standing cyclonic eddies in the region, particularly during the month of August. When flow moving towards the sill reaches lower depths, it is forced to develop anticyclonic circulation in order to conserve its potential vorticity. Cyclonic eddies may form when that same flow reaches deep water on the other side of the sill. In order to compensate for the rapid change in depth, the flow is then forced to develop cyclonic circulation that can be significantly strengthened by that same drastic depth increase. These eddies can last for a period of 30-40 days, which forces a flow pattern during their

lifespan: flow to the north on the east side of the MP and to the south on the west side. In the context of Baums et al. (2006)'s paper, this flow pattern may constitute a physical barrier that limits the transport of coral larvae from the eastern side of the Passage to the western side.

Part of the question we aim to answer with this study is which oceanographic phenomena control the surface currents in the MP region. Surface currents properties can be inferred from Lagrangian drifter trajectories. Taken together, the drifter trajectories described in **Section 4.1.2** provide a unique data set that reveals details of the circulation patterns in the MP.

During February 2015, the first four drifters (#3 to #6) followed a northwestward trend and crossed the MP in less than two weeks. See top left panel from **Fig. 4.3**. There were very distinct oscillations visible in the path of these first drifters, and these oscillations seemed to be a direct result of tidal forcing. These and a couple of other drifter trajectories are analyzed in **Section 4.3.4** to corroborate the presence of tidal flows. Another drifter (#7), deployed almost a week after the initial four, followed a southwestward trend towards Mona Island, but after passing to the south of this island, it moved northward. In mid-March 2015, a mesoscale eddy passing to the south of PR and Hispaniola carried southward the three drifters (#8 to #10) that were deployed at that time (#8 and #9 at Bajo de Sico; #10 at LP). **Fig. 4.10** shows an overlay of the drifter trajectories on top of contours of satellite-derived altimetry, providing clear evidence of the impact of mesoscale structures on the coastal circulation off western PR. In early April 2015, one drifter (#12) deployed to the southeast of PR and moving westward reached the MP. In late April 2015, four more drifters (#13 to #16) were deployed at Bajo de Sico and moved straight northward and then eastward after passing to the northwest of PR.

4.3.2 Mesoscale eddies

The connectivity between large-scale ocean phenomena and the MP's flow patterns had been briefly mentioned in Baums et al. (2006), who indicate that the flow pattern of the MP “*can be strongly perturbed by large-scale eddies on either side of the Passage [North or South side], and they will then force southward or northward flow through the entire width of the Passage.*” The drifter tracks shown in **Fig. 4.10** demonstrate that mesoscale eddies are capable of pulling water masses from close to La Parguera and the Mona Passage towards the south and well into the Caribbean Sea. The color bar indicates sea surface height anomaly based on satellite-derived altimetry measurements. The presence of an anticyclonic eddy, which causes an increase in the sea surface height anomaly, is highlighted by the darker red tones. This serves as evidence that the waters within the MP can be strongly influenced by large scale phenomena advancing through the Caribbean Sea. The behavior of these drifters proves that large-scale ocean phenomena can strongly impact the coastal circulation in the Mayagüez (western PR) shelf. This is the first time that the susceptibility of the MP to passing mesoscale eddies to the south of the Passage has been observed.

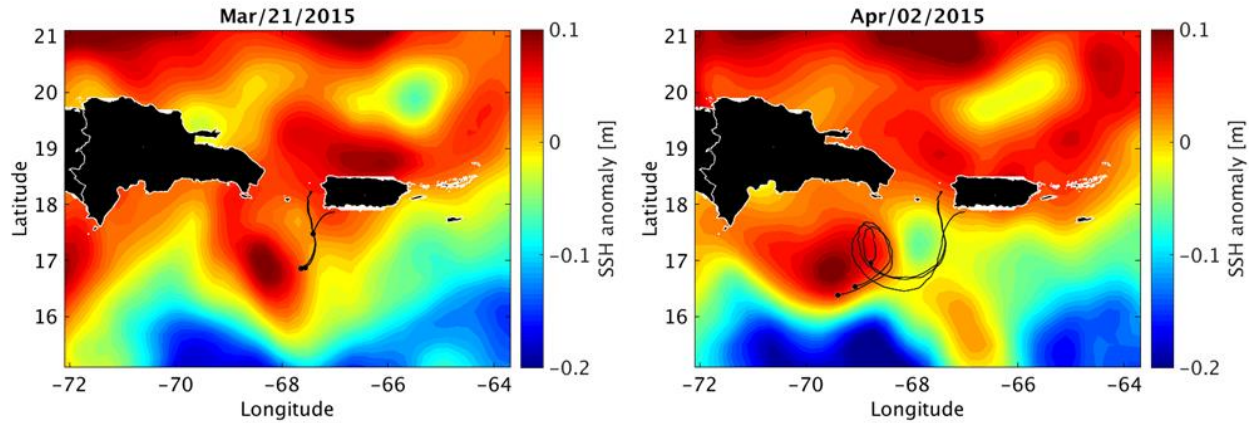


Fig. 4.10 Progression of PVC drifters (#8, #9, and #10) as they were entrained in a mesoscale anticyclonic eddy. Color bar indicates sea surface height anomaly (above geoid) in meters. Data courtesy of CoastWatch Caribb-NOAA AOML PhD.

4.3.3 Tidal flows

Tides are predominantly semidiurnal for the North Atlantic Ocean, but mostly diurnal for the northeastern Caribbean Sea, a result of the presence (existence) of amphidromic points for semidiurnal tidal constituents, M2 and S2, in the Eastern Caribbean (Kjerfve 1981; Ricardo 2011; Zetler and Cummings 1972). Due to its proximity to these amphidromes, the MP is a transition area characterized by mixed tides. The periodic changes in the drifter velocity time series shown in **Fig. 4.7** and **Fig. 4.8** suggest that the drifter trajectories are sensitive to tidal fluctuations. In the following section we conduct spectral analysis to determine the periodicity of these oscillations.

4.3.4 Spectral analysis

The time series of the velocity components of surface drifters were studied through a Short-Time Fourier Transform (STFT) analysis to determine the dominant oscillation periods in the drifter velocity time series. One drifter, ECO #1, is used here as the case study for the spectral analysis. ECO #1 was deployed on April 26, 2017, at approximately 7 miles off the coast of LP,

located in the south coast of PR. The top left panel in **Fig. 4.11** shows the trajectory of this drifter which travelled northward during the first few hours, then westward until it reached the southwestern most corner of PR. After that point, the drifter entered the MP and crossed the Passage in a northwestward direction within six days, changing its course to the southwest after reaching latitude 19.4°N . After reaching a minimum distance of 5 miles off the coast of the DR, the drifter followed a northwestward current along the northern DR's coastline for five more days, with its last position being recorded on May 18, 2017.

The top right panel in **Fig. 4.11** shows the drifter trajectory in colors corresponding to the instantaneous drifter speed. The numbers over the drifter tracks indicate the day after deployment that the drifter reached the end of each region: day 2 for the south of LP, day 7 for the MP, and day 20 for the north of the DR. The regions in which the drifter experienced the strongest surface currents can be easily identified in this plot: midway along the MP and after heading towards the DR's northern coastline. Slight oscillatory movements along the drifter's track can be appreciated as well.

The middle left panel and middle right panels in **Fig. 4.11** show the time series for the u and v components of the drifter velocity, respectively. The gray shading indicates the approximate region in which the drifter was located: from 0-2 days south of the LP, from 2-7 days inside the MP, and from 7-20 days north of the DR. These regions are known for being dominated by different tidal cycles: LP region, located to the south of PR, is characterized by a diurnal tide cycle; the MP, by a mixed tide cycle with a stronger influence from the diurnal tide cycle; while the semidiurnal tide dominates off northern DR.

The bottom left panel and bottom right panels on **Fig. 4.11** show the results of the STFT spectral analysis for the u and v components of the drifter velocity, respectively. The semidiurnal

frequencies clearly dominate the drifter dynamics within the MP (days 2-7), and while there is still significant energy in the semidiurnal tide after day 7, other low frequency phenomena start to dominate the signal. From this analysis, it is clear that the drifters were subject to very heterogeneous tidal forcing along their trajectories.

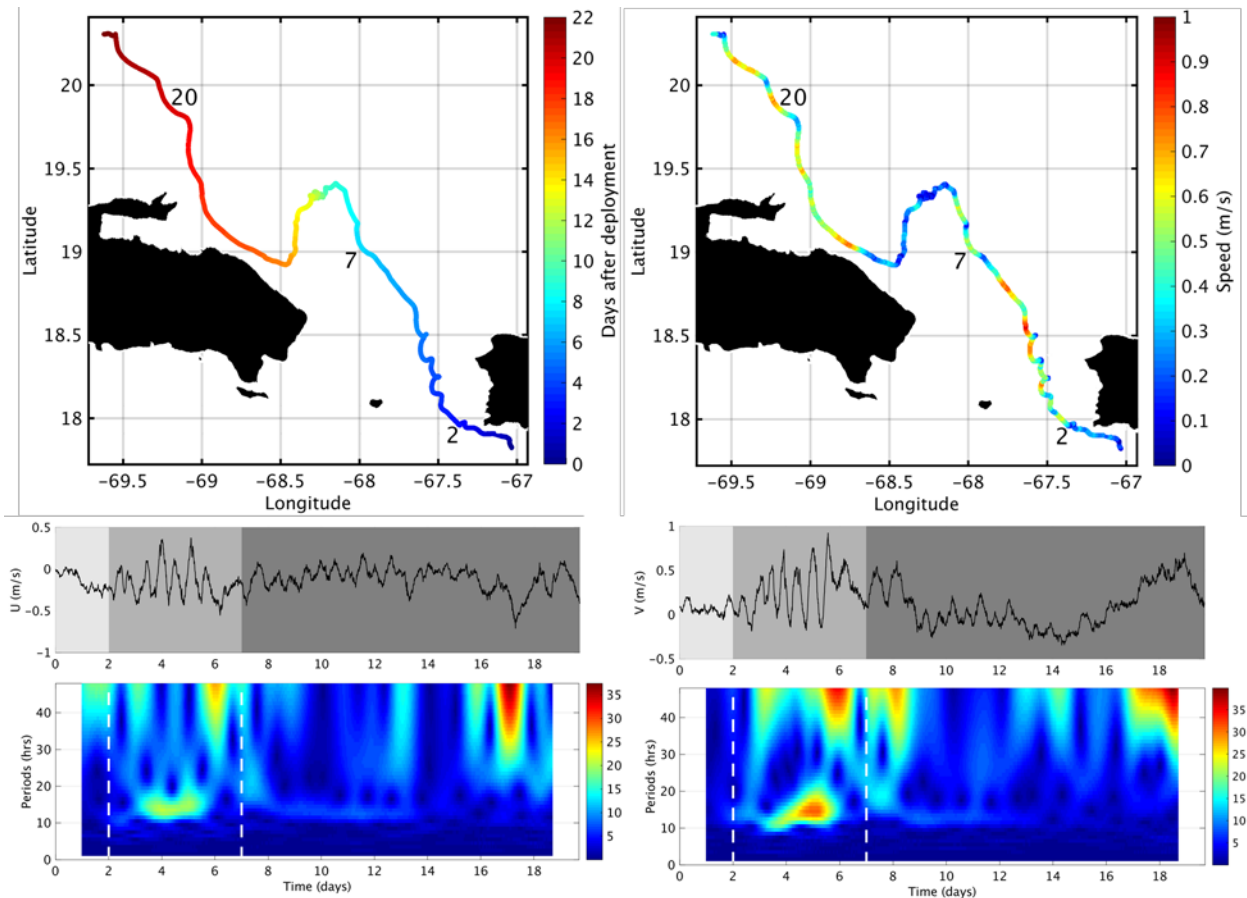


Fig. 4.11 [top panel] Track with number of days after deployment (left), and velocity magnitude (right) corresponding to each drifter position. In both plots, DR to the left, PR to the right. [middle panel] U (left) and V (left) time series sectioned by region. The bounding boxes indicate the regions entered by the drifter: [1:2 days after deployment] = LP, [2:7] = MP, [7:20] = Northern DR [20:22] = Offshore DR [bottom panel] STFT results for the entire u (left) and v (right) time series using a 48-hr sample window with a 42-hr overlap.

4.4 Lagrangian dispersion

Lagrangian drifters are the only instruments capable of adequately observing dispersion in the upper ocean (Lumpkin 2016). This section will be dedicated to the analysis of lateral dispersion processes dominating the MP using data from the ECO drifter deployments.

The distance between an object and its original position at a given moment in time is called absolute separation, while the distance between two objects at a moment in time is called relative separation. Both quantities are measured in units of length (L) and should not be confused as measures of dispersion. Mean drift (M) is defined as the separation of the center of mass of a cluster of drifters from its initial position, which makes it an analogous measure of absolute separation for drifter clusters. Lateral dispersion (D_L) is defined as the measure of spatial extent, in two dimensions, covered by an object. It measures how spread out the object is from its original position (absolute dispersion) or from another object (relative dispersion) in units of squared length (L^2). These flow properties are important for a vast range of applications such as sedimentation in estuaries and rivers, the dynamics of plankton in the ocean, deep-sea landslides, and the dynamics and collisions of water droplets in clouds (Gibert et al. 2010). Absolute dispersion is relevant when it comes to larval connectivity studies, where the goal is to know how far larvae travels from its spawning site before it settles, while relative dispersion, or two-point dispersion, plays a fundamental role in understanding the speed and spreading rate of the patches of pollutants (Poje et al. 2014).

Pair separation distance will determine the spatial and temporal scales of the phenomena that will influence pair separation and, subsequently pair dispersion and pair dispersion rates. The space-filling configuration of the nodes used for the ECO drifter deployment and the initial separation distances of 100-m and 2-km enabled the drifters to provide measurements of dispersion

at the submesoscale (100 meters to tens of kilometers). After the drifters reached separation distances of over 10 km, measuring dispersion at the mesoscale (spatial scales larger than 10 kilometers) was made possible as well.

4.4.1 Absolute dispersion

Absolute separation is determined here through the quantification of the mean drift of each drifter cluster. The mean drift quantifies the displacement of the center of mass along any chosen direction, for example, in the x -direction (zonal):

$$M_x(t) = \frac{1}{N} \sum_{i=1}^N [x_i(t) - x_i(0)]. \quad (\text{LaCasce 2008})$$

The top plot in **Fig. 4.12** shows the zonal mean drift (M_x) for the T1 and T2 releases. In all plots, T1 results are presented in blue; T2, in black. The second plot shows the meridional mean drift (M_y) for the same releases. The magnitude and direction of the mean drifts, M_{T1} and M_{T2} , are shown as vectors in the bottom two panels of **Fig. 4.12**. The increase in mean drift numerically represents how far the centroid of each cluster travelled from its deployment site. In general, the zonal and meridional mean drifts of both deployments were very similar during the first 10 days, with drift rates of about 20 km/day. After day 10, the T1 cluster continued with a similar mean drift rate while the T2 cluster's drift slowed down, resulting in a much larger overall drift for T1 after 18 days.

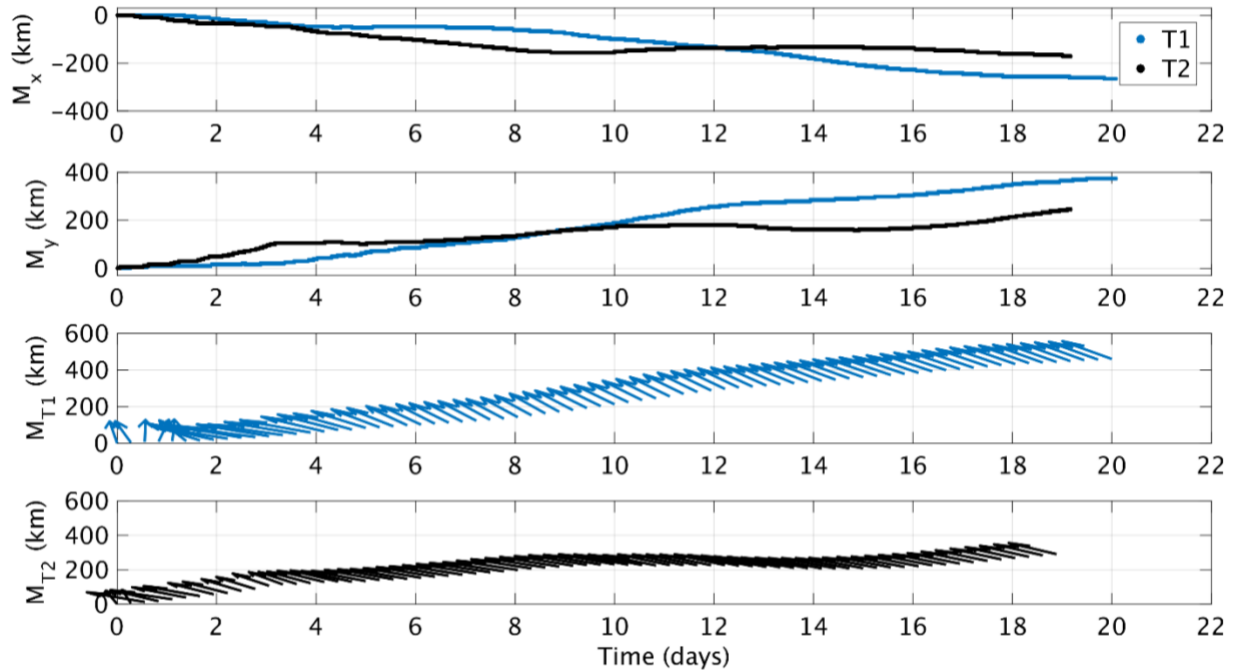


Fig. 4.12 Mean drift results for both nodes (triangles), T1 and T2, released as part of the ECO drifter deployment. [top] Zonal mean drift comparison (negative (-) indicates westward movement). [middle top] Meridional mean drift comparison. [middle bottom] Directions of the mean drifts of T1 positioned at their magnitude values. [bottom] Directions of the mean drifts of T2 positioned at their magnitude values. T1 results shown in blue; T2, in black.

4.4.2 Relative dispersion

The absolute separation results presented in the previous section analyzed the separation of the center of mass of clusters from their original locations, but the drifter pairs and the groups of three drifters enable the quantification of relative dispersion and an analysis of the scale dependence of pair separation rates. **Fig. 4.13** shows the trajectories of the drifters in each cluster, color coded by drifter number. Note that when drifters reach the north of the MP their separation seems to increase greatly.

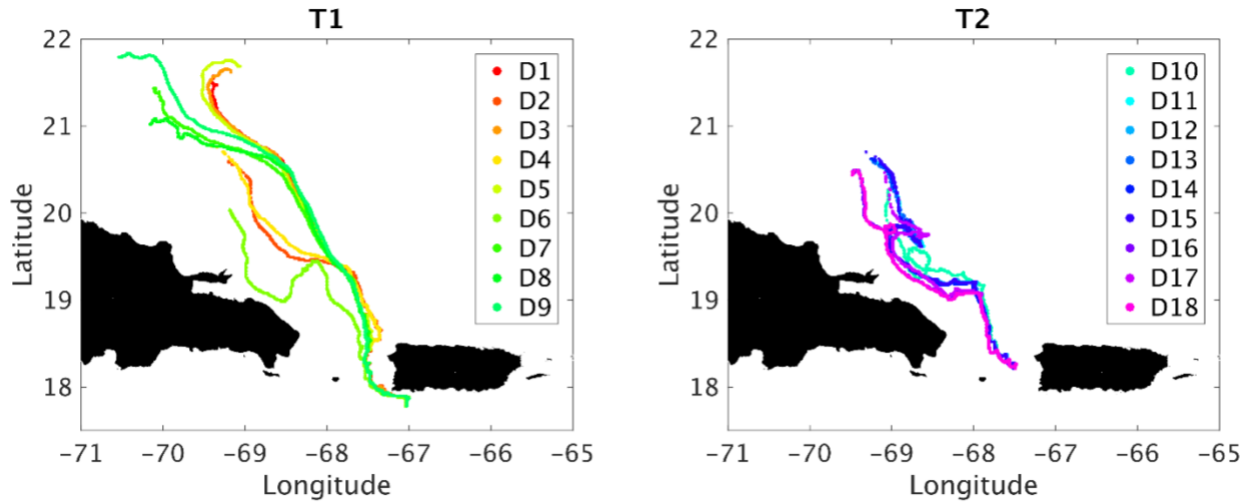


Fig. 4.13 Visual representation of the difference in spatial spreading between the two nodes deployed on April 2017.

Fig. 4.14 shows the temporal evolution of the number of drifter pairs at given separation distances for the T1 (top), and T2 (bottom) releases. Note the higher concentration of drifter pairs that remain closely united (separation distances shorter than 250 meters) during a longer period (0 to 6 days) for the T1 release. This indicates that large numbers of contemporaneous drifter pairs, especially at the submesoscale, were obtained for cluster T1, which is a very similar result to the one published by Poje et al. (2014) for deployments within the Gulf of Mexico. In contrast, the pairs of drifters released in the MP (T2 release) seem to disperse much more quickly, leaving only one pair with a separation distance of less than 250 meters during day 6. T2 drifter pairs remained under a separation distance of 100 km at all times, but some of the T1 drifter pairs obtained separation distances of 100 km or more in just 10 days after deployment.

The T1 cluster experienced a progressive increase in pair separation distances. During the first 6 days after deployment, relative separation was restricted to the submesoscale for the T1 drifters since pair separation ranged from 100m to 10 km. After those first 6 days, some drifter

pairs became susceptible to the influence of larger scale phenomena, and, by the end of the time series, all pair separation distances were out of the submesoscale range. The T2 cluster behaved differently. After just 2 days after deployment, some of the drifter pairs from this cluster became susceptible to the influence of larger scale phenomena, but this did not result in all pair separations eventually exiting the submesoscale range. As a matter of fact, the contrary turned out to happen: by the twenty-second day, most of the T2 cluster's pair separations were still being exclusively influenced by submesoscale processes because most of the separation distances were still well below the 10-km threshold.

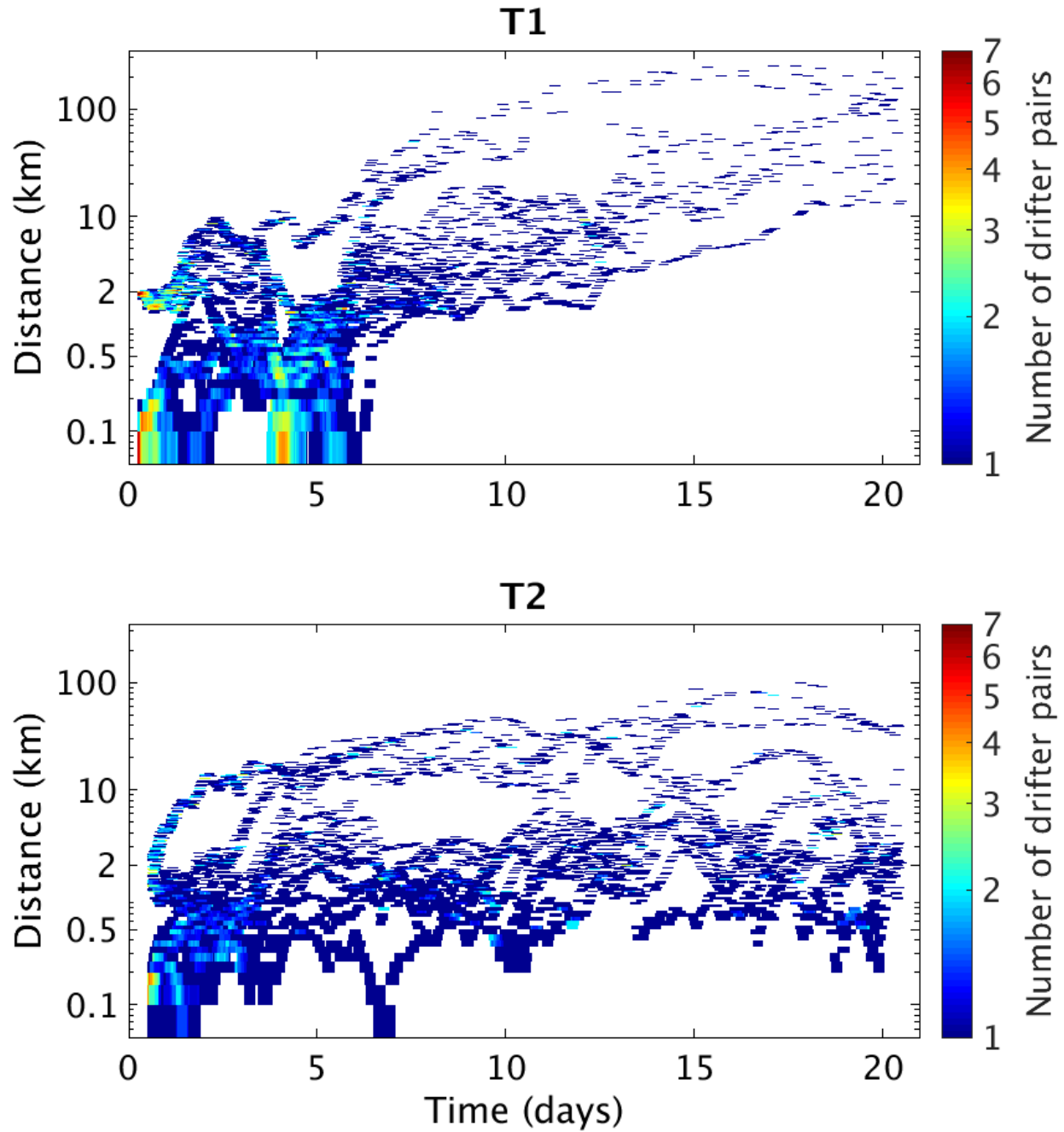


Fig. 4.14 Time evolution of the number of drifter pairs at given separation distances for the T1 (top), and T2 (bottom) releases (T1 = triangle released south of LP, T2 = triangle released within the MP). Increments at 50 m along the y-axis and 1-hr intervals along the x-axis. Data smoothed over 6-hr intervals.

For individual drifter pairs, relative dispersion can be directly computed as the time dependent mean square pair separation (Ohlmann et al. 2012). For drifter clusters, cloud variance

or cloud spreading presents another measurement of relative dispersion. Cloud variance, D , represents the spread about the center of mass of the cluster and it can be quantified by the variance of the drifter displacements. As an example, the zonal cloud spreading was defined as:

$$D_x(t) = \frac{1}{N-1} \sum_{i=1}^N [x_i(t) - x_i(0) - M_x(t)]^2. \text{ (LaCasce 2008)}$$

Fig. 4.15 shows the cloud variance time series for both nodes, T1 and T2. The cumulative spreading about the center of mass is larger for T1 when compared to T2, especially after day 7.

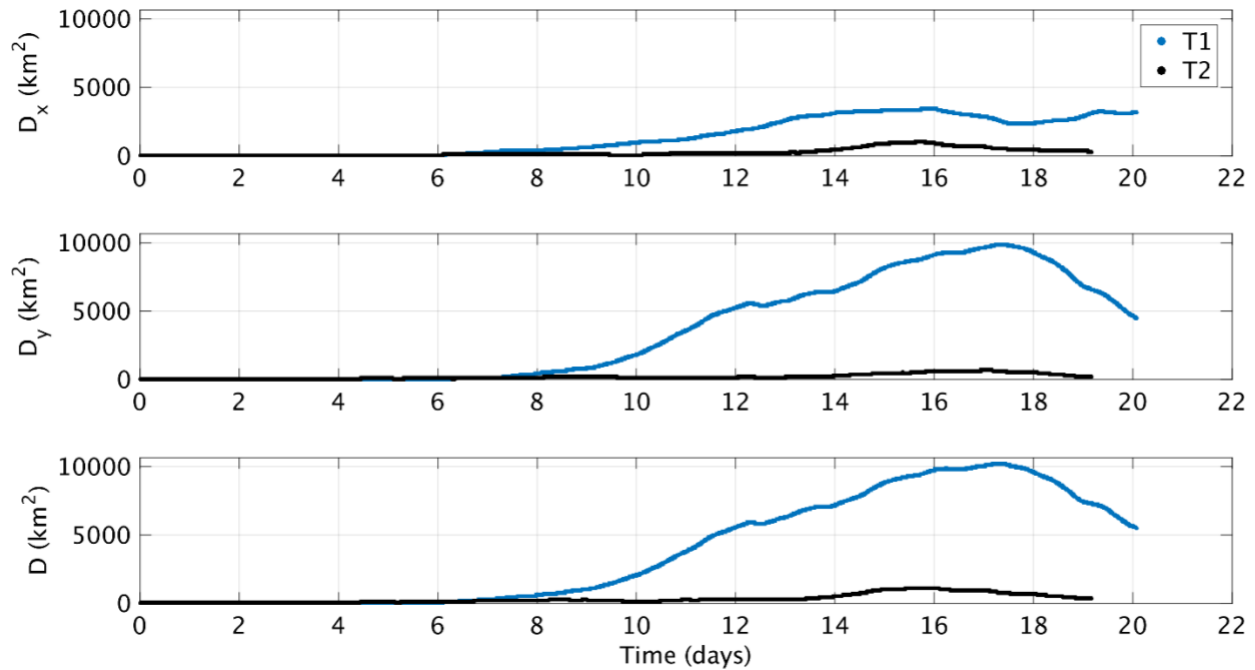


Fig. 4.15 Time series of cloud variance [top] along zonal direction, (D_x) and [middle] along meridional direction, (D_y), for T1 and T2 releases. [bottom] Time series of magnitude of the cloud variance, D , for T1 and T2 releases. T1 shown in blue; T2. Particularly after day 7, spreading was significantly larger for LP (T1), than for MP (T2).

This period of seven days encompasses the amount of time the drifters spent within the MP, which visually suggests drifter clusters experienced less spreading within the MP than outside of it. But cloud variance results are very sensitive to outliers in the form of drifter paths that have

deviated far from the cluster's average track, such as the path of ECO #6 in **Fig. 4.13**. To be able to discern whether or not there is actually a significant difference between the spreading of these two clusters, it is necessary to compute the scale-dependent dispersion rates. Based on Poje et al. (2014), the statistical quantities of interest for dispersion rates are the scale-dependent relative dispersion $D^2(t) = \langle \mathbf{D} \cdot \mathbf{D} \rangle$ (where the $\langle \ \rangle$ operator indicates an average over particle pairs and \mathbf{D} denotes the pair separation vector) and the average separation velocity, $\Delta v(r)$, at a given separation distance, r . The relative dispersion rate will be given by the time-scale $\lambda(r) = \Delta v(r)/r$. The velocity scale is defined by $\Delta v(r) = \sqrt{\langle \delta v^2 \rangle}$, where δv^2 is the square velocity of separation between drifter pairs and is defined by $\delta v^2 = \delta \mathbf{v}_{ij}^2(t) = \left(\frac{d\mathbf{D}_{ij}}{dt}(t) \right)^2$, following the notation described in Ohlmann et al. (2012). \mathbf{D}_{ij} represents the separation distance vector between drifters denoted by i and j . The i index ranges from 1 to 8 (10 to 17) and the j index, from 2 to 9 (11 to 18) generating the 36 drifter pairs resulting from the T1 (T2) deployment. The δv^2 values were computed for all drifter pairs, and binned, in logarithmic scale increments, by pair separation distance. **Fig. 4.16** shows the mean δv^2 as a function of the pair separation, r .

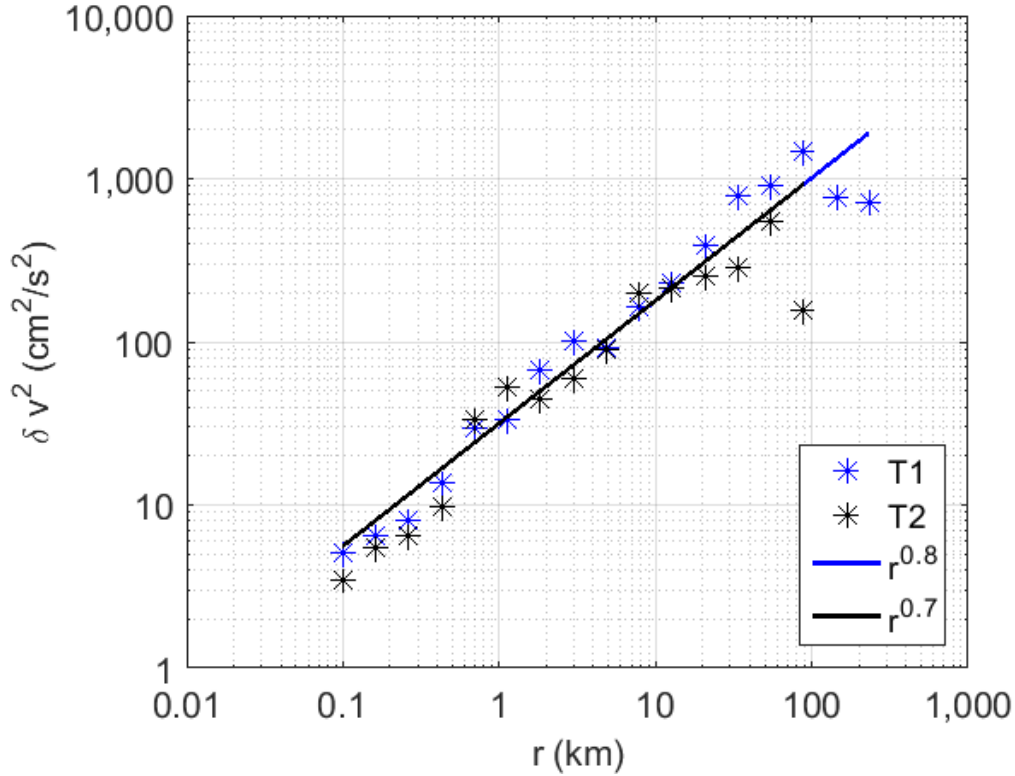


Fig. 4.16 Mean square relative velocity as a function of pair separation. The solid lines indicate the best polynomial fit for the same colored data set. The blue and black symbols represent T1 and T2 results, respectively.

For all pairs in cluster T1, values of mean square separation velocity range from $5 \text{ cm}^2/\text{s}^2$ for the 100-162.4 m bin, to $1600 \text{ cm}^2/\text{s}^2$ for the 143.8-233.6 km bin. Values of δv^2 computed from all available drifter pairs in cluster T2 range from $3.5 \text{ cm}^2/\text{s}^2$ for the 100.0-162.4 m bin, to $600 \text{ cm}^2/\text{s}^2$ for the 88.6-143.8 km bin. These results show an exponential increase with length scale for the separation velocities of both clusters. This length scale dependency is in agreement with observations from Ohlmann et al. (2012), where, on average, drifter pairs accelerated from one another as their relative velocities grew with increasing separation distance.

From **Fig. 4.16**, a scale dependence of separation velocity on particle separation distance is evident. As the particle separation, r , increases, the separation velocity also increases, at least for

scales smaller than 100 km. For these scales these results agree with the assumption from turbulence theory stating that larger scales of turbulence are more energetic, and consequently, provoke (induce) larger separation velocities. This scale dependence of the velocity of separation on D holds true for both clusters, T1 and T2. For scales of around 100 km for the T2 cluster and for scales larger than 100 km for the T1 cluster there is a decrease in the separation velocity.

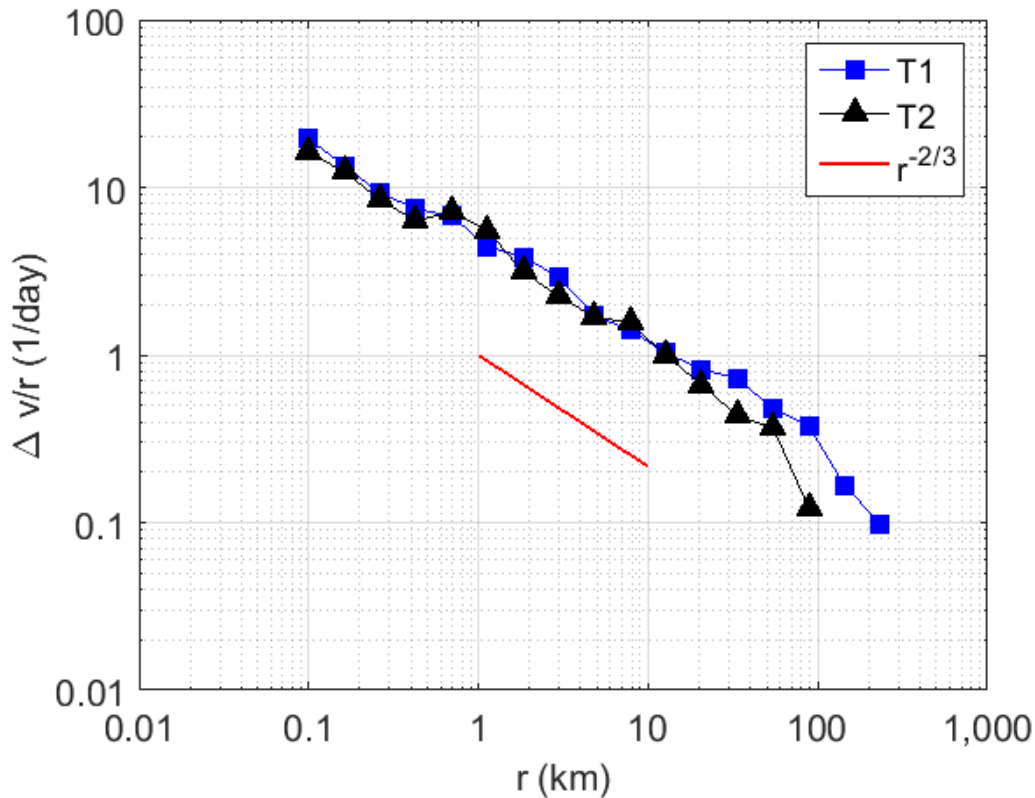


Fig. 4.17 Scale dependent pair separation rate, or relative dispersion rate, as a function of separation distance, r , for the T1 (in blue) and T2 (in black) deployments.

Taking the square root of the resulting values of δv^2 and dividing it by the pair separation distance, r , yields a scale-dependent pair separation rate as a function of r (see **Fig. 4.17**). For both clusters, the dispersion rate results indicate that faster separation rates correspond to smaller separation distances. These pair separation rates, given by $\lambda(r)$, compare (scale) rather well

with $r^{-\beta}$, $\beta \neq 0$ for separation scales between 100 m and 10 km, although there is a small bump at scales of 700m, which may be due to the fact that the primary triangles of the cluster arrangements were separated at 700m. For these scales, the resulting exponents from both clusters are consistent with Richardson's two-thirds law. As separation distance increases, the time-scale decreases, meaning that the relative dispersion rate decreases as well. The results presented in **Fig. 4.17** are consistent with the results published by Poje et al. (2014), who analyzed scale separation rates for three clusters consisting each of about 90 drifters deployed with initial separation distances ranging from 100 m to 2 km.

As previously mentioned, an important motivation behind this project was being able to provide reliable estimates of dispersion coefficients or, better said, diffusivity estimates. **Fig 4.18** shows the effective diffusivity results from both cluster releases, T1 and T2. As shown in this figure, the results from both clusters align very well with each other and follow an exponential trend around the value of $r^{1.35}$.

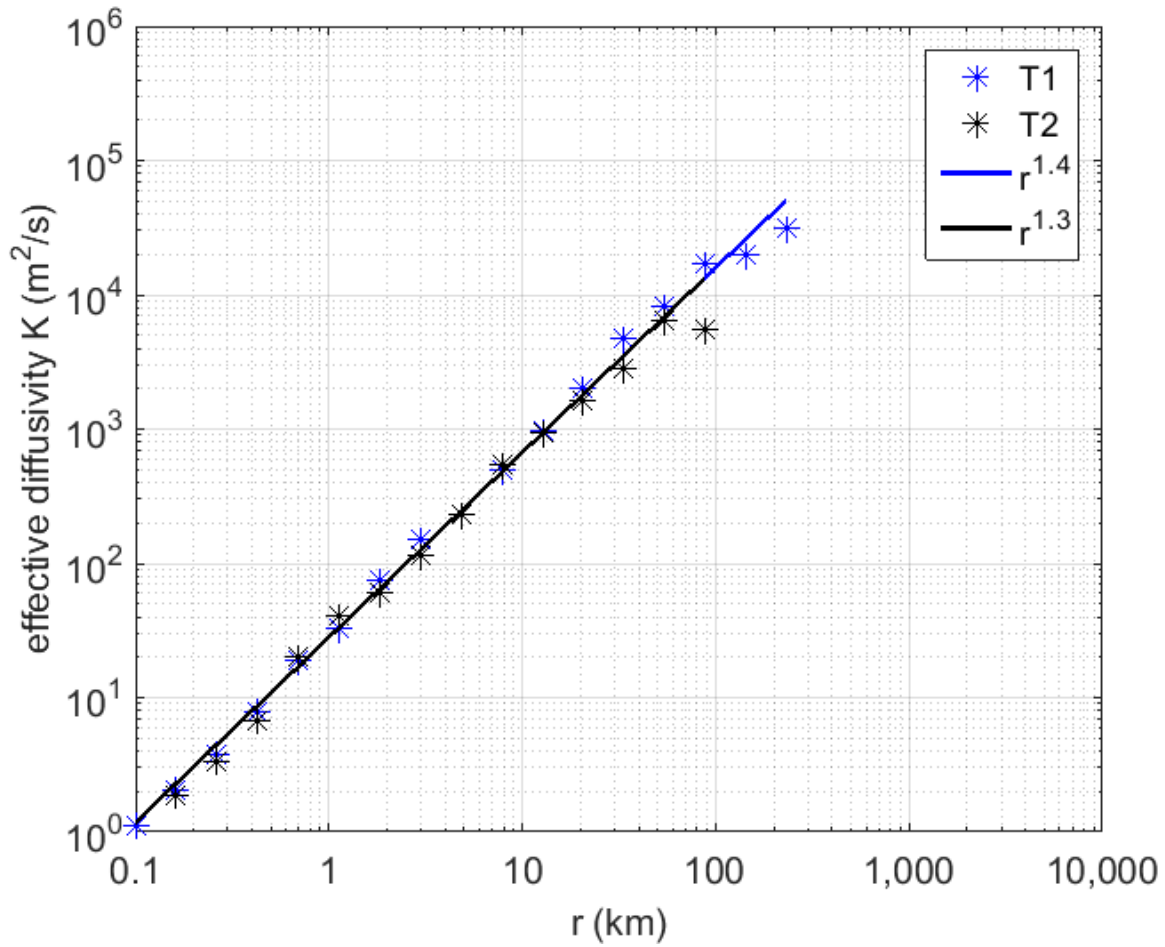


Fig 4.18 Effective diffusivity as a function of separation distances. Fixed-scale average $K(r)$ vs separation distance (r) for the T1 (in blue) and T2 (in black) deployments.

Chapter 5

Discussion and conclusions

Inexpensive GPS-tracked drifters have been used to elucidate some important aspects of the near-surface circulation in the Mona Passage and off southwestern PR. A comparison between HF Radar-derived velocities and drifter-based estimates demonstrates that these CODE-inspired drifter designs correctly follow the surface current patterns in the region. Drifter trajectories from an April 2015 deployment showed the impacts of a mesoscale eddy in coastal circulation, highlighting the connectivity between shelf waters off western PR and the open ocean. A spectral analysis of drifter velocities showed that the semidiurnal tidal oscillations clearly dominate the drifter dynamics within the MP, and, while there is still significant energy in the semidiurnal tide after exiting the MP, other low frequency phenomena start to dominate the signal.

Two near-simultaneous drifter cluster deployments were conducted, following the arrangement strategy used by Poje et al. (2014) which allows for multi-scale observations of drifter dispersion dynamics. The initial release locations of each cluster were subject to very different hydrodynamic forcing mechanisms: the T1 cluster was released off southwestern PR where tidal forcing is minimal, while the T2 cluster was released in the midst of the Mona Passage where semidiurnal tidal forcing dominates. However, after 3 days the T1 cluster was advected into the MP, very close to the release location of the T2 cluster, thus sampling the same hydrodynamic regime, but with different initial conditions and drifter spacing since the T1 cluster had already been drifting for several days.

It is important to discuss the different spatial scales affecting the flow dynamics sampled by these drifters. The first baroclinic Rossby radius of deformation for the region is between 60-70 km (Chelton et al. 1998), and significant submesoscale eddies have been observed using HF radar off southwestern PR (Pomales-Velazquez et al. 2015) near where the T1 cluster was released. The width of the Mona Passage, as measured from the western coast of Puerto Rico to the eastern coast of the Dominican Republic is about 100 km. However, the shelf extends from 5-25 km on either side, with topographic features such as seamounts and Mona Island occurring in between. This complexity will likely limit the cross-channel scales of any coherent structures to a maximum of a few tens of kilometers.

Cloud variance, a relative dispersion measure for drifter clusters, was observed to be much larger for T1 when compared to T2. The drastic increase in cloud variance occurred, for both clusters, right around the time each cluster reached waters outside of the MP, which could indicate that water masses exhibit less dispersion within the MP than outside of it. However, care should be taken with this conclusion since the scale-dependent relative dispersion rate for both clusters is very similar as shown by the scale-dependent pair separation rate results. This indicates that the drastically different cloud variance results obtained for T1 are most likely a result of the cumulative spreading of drifter pairs after the passing of ~20 days, and, perhaps, the clusters' interaction with a stronger mean flow than the one observed for T1.

The scale dependence of separation velocity on particle separation distance was analyzed through the square relative velocity vector between drifter pairs. An exponential growth, in the mean square relative velocity values, can be observed with pair separation distance. The relative velocity ranged from 5 to ~1600 cm^2/s^2 (3.5 to 600 cm^2/s^2) over length scales from ~100 m to 350 km (~100 m to 100 km) for the T1 (T2) cluster. For both clusters, the mean square relative velocity

increases as the pair separation increases. This length scale dependency is in agreement with standard turbulence theory: that the separation velocity of particles undergoing relative dispersion can accelerate as particle separation distance increases (Ohlmann et al. 2012).

In Ohlmann et al. (2012), the mean square relative velocity, as a function of pair separation, fit to a $r^{0.9}$ curve (line) for data from 1-2 days tracks sampled every 10 minutes with initial separations of 5-10 meters, which meant that their separation distance spanned from 5 m to 4 km, which is a smaller range than ours (100 m to 350 km). But with our mean square separation velocity results fitting to $r^{0.8}$ and $r^{0.7}$ curves (lines), for clusters T1 and T2, respectively, it can be seen that our values compare well with the results from this previously published work. The fact that our results are so similar, for such different separation scales, indicates that the magnitudes of the δv^2 values based on our in-house drifter design are very consistent with other drifter-based δv^2 observations, and extend the $\delta v^2(r) \sim r^{0.9}$ scaling to larger scales.

Our relative dispersion rate compares favorably with the ones published by Poje et al. (2014), and clearly indicates that faster growth rates correspond to smaller separations, independently of the deployment site (cluster). For both sets of drifter data, Poje et al. (2014)'s and ours, as separation distance increases, the drifter pairs experience significantly smaller dispersion rates, and the scale-dependent dispersion results scale well with $r^{-2/3}$, for separation scales below 10 km, consistent with Richardson's two-thirds law.

Very similar results for the scale-dependent pair separation rate for scales smaller than 10 km were obtained for both clusters (T1 and T2). Since both clusters travelled through the same region, by a difference in time of just about two and three days, depending on the chosen drifters, a similarity between relative dispersion rates was expected. These results suggest that the MP and the region off southwestern PR can be characterized by similar scale-dependent relative dispersion

rates at scales smaller than 10 km. For scales of around 100 km and above, when drifters exited the MP, a significant difference in both the separation velocity and the scale-dependent separation rate was found for both clusters, although the T2 cluster did not sample scales larger than 100 km. The cumulative impact of these different separation rates at the mesoscale led to the dramatic difference in the cloud dispersion shown in **Fig. 4.15**. It is difficult to pinpoint the exact reasons for the difference in separation rates, but since both clusters exhibited the same separation rates for small scales, the influence of the release location can be ruled out. The only plausible explanation is that both clusters exited the Mona Passage at different times, causing the T1 cluster to become embedded in a stronger mean flow, causing the cluster to travel farther north than the T2 cluster which stayed closer to the north coast of the DR, thus experiencing different oceanographic dynamics.

From **Fig. 4.18**, we can estimate what the diffusivity coefficient should be for a model with a grid size of 10 km: it should be no less than $600 \text{ m}^2/\text{s}$ in order to allow the model to solve processes occurring at smaller scales than its grid size. For a model with a grid size of 500 m, the effective diffusivity should be no less than $10 \text{ m}^2/\text{s}$. But we must be careful with this approximation, the fact that a model has a 10 km resolution, does not ensure that the model can correctly resolve processes occurring at that scale. The relation between a model's grid size and its resolution depends on the type of model, it depends on whether it solves the hydrodynamics of a particular region over a regular grid or over an unstructured domain.

The results presented herein are the first direct estimates of small-scale particle dispersion in and around the Mona Passage. As evidence by the pair separation rate results, both submesoscale (100 m to 10 km) and mesoscale (larger than 10 km) spatial scales of motion play a significant role in the surface circulation of waters north and inside the MP and the waters to the southwest of

PR. Existing operational circulation models for the region have spatial resolution ranging from 1-3 km. The results of this study provide an important dataset that will allow for the calibration of the simulated scale-dependent dispersion characteristics of these models. This data will also be useful to understand the impact of the small scale (subgrid) motions not directly resolved by these models on their performance metrics.

References

- Aponte-Bermúdez LD, Rodríguez-Romero HJ, Morell JM, Rodríguez E (2015) CARICOOS: Improving high-resolution numerical weather prediction for the northeast Caribbean region. OCEANS 2015 - MTS/IEEE Washington.
<https://doi.org/10.23919/OCEANS.2015.7404498>
- Assireu AT, Stevenson MR, Stech JL (2003) Surface circulation and kinetic energy in the SW Atlantic obtained by drifters. *Continental Shelf Research* 23:145-157.
[https://doi/10.1016/s0278-4343\(02\)00190-5](https://doi/10.1016/s0278-4343(02)00190-5)
- Baums IB, Paris CB, Chérubin LM (2006) A bio-oceanographic filter to larval dispersal in a reef-building coral. *Limnology and Oceanography* 51:1969-1981.
<https://doi/10.4319/lo.2006.51.5.1969>
- Berti S, Santos FAD, Lacorata G, Vulpiani A (2011) Lagrangian Drifter Dispersion in the Southwestern Atlantic Ocean. *Journal of Physical Oceanography* 41:1659-1672.
<https://doi/10.1175/2011jpo4541.1uu>
- Chelton DB, deSzoek RA, Schlax MG, et al (1998) Geographical Variability of the First Baroclinic Rossby Radius of Deformation. *Journal of Physical Oceanography* 28:433-460. [https://doi.org/10.1175/1520-0485\(1998\)028<0433:gvotfb>2.0.co;2](https://doi.org/10.1175/1520-0485(1998)028<0433:gvotfb>2.0.co;2)
- Davis RE (1985) Drifter observations of coastal surface currents during CODE - The method and descriptive view. *Journal of Geophysical Research* 90:4741-4755.
<https://doi.org/10.1029/jc090ic03p04741>

- Gibert M, Xu H., Bodenschatz E (2010) Inertial effects on two-particle relative dispersion in turbulent flows. *EPL (Europhysics Letters)*. <https://doi.org/10.1209/0295-5075/90/64005>.
- Johns WE, Townsend TL, Fratantoni DM, Wilson WD (2002) On the Atlantic inflow to the Caribbean Sea. *Deep Sea Research Part I: Oceanographic Research Papers* 49:211–243. [https://doi.org/10.1016/s0967-0637\(01\)00041-3](https://doi.org/10.1016/s0967-0637(01)00041-3)
- Kjerfve B (1981) Tides of the Caribbean Sea. *Journal of Geophysical Research* 86:4243-4247. <https://doi.org/10.1029/jc086ic05p04243>
- LaCasce JH (2008) Statistics from Lagrangian observations. *Progress in Oceanography* 77:1–29. <https://doi.org/10.1016/j.pocean.2008.02.002>
- Lumpkin R, Özgökmen T, Centurioni L (2017) Advances in the Application of Surface Drifters. *Annual Review of Marine Science* 9:59–81. <https://doi.org/10.1146/annurev-marine-010816-060641>
- Niiler PP, Sybrandy AS, Bi K et al (1995) Measurements of the water-following capability of holey-sock and TRISTAR drifters. *Deep Sea Research Part I: Oceanographic Research Papers* 42:1951–1964. [https://doi.org/10.1016/0967-0637\(95\)00076-3](https://doi.org/10.1016/0967-0637(95)00076-3)
- Ohlmann JC, Lacasce JH, Washburn L, et al (2012) Relative dispersion observations and trajectory modeling in the Santa Barbara Channel. *Journal of Geophysical Research*. <https://doi.org/10.1029/2011jc007810>
- Poje AC, Ozgokmen TM, Lipphardt BL, Haus BK, Ryan EH, Haza AC et al (2014) Submesoscale dispersion in the vicinity of the Deepwater Horizon spill. *Proceedings of the National Academy of Sciences (PNAS)* 111:12693-12698. <https://doi.org/10.1073/pnas.1402452111>

- Pomales-Velazquez L, Morell JM, Rodriguez-Abudo S, et al (2015) Characterization of mesoscale eddies and detection of submesoscale eddies derived from satellite imagery and HF radar off the coast of southwestern Puerto Rico. OCEANS 2015 - MTS/IEEE Washington. <https://doi.org/10.23919/oceans.2015.7404612>
- Poulain P-M (2001) Adriatic Sea surface circulation as derived from drifter data between 1990 and 1999. *Journal of Marine Systems* 29:3–32. [https://doi.org/10.1016/s0924-7963\(01\)00007-0](https://doi.org/10.1016/s0924-7963(01)00007-0)
- Poulain P-M, Gerin R, Mauri E, Pennel R (2009) Wind effects on drogued and undrogued drifters in the Eastern Mediterranean. *Journal of Atmospheric and Oceanic Technology* 26:1144-1156. <https://doi.org/10.1175/2008jtech0618.1>
- Richardson LF (1926) Atmospheric Diffusion Shown on a Distance-Neighbour Graph. *Proceedings of the Royal Society A: Mathematical, Physical and Engineering Sciences* 110:709-737. <https://doi.org/10.1098/rspa.1926.0043>
- Richardson PL (2005) Caribbean Current and eddies as observed by surface drifters. *Deep Sea Research Part II: Topical Studies in Oceanography* 52:429-463. <https://doi.org/10.1016/j.dsr2.2004.11.001>
- Salazar JP, Collins LR (2009) Two-Particle Dispersion in Isotropic Turbulent Flows. *Annual Review of Fluid Mechanics* 41:405-432. <https://doi.org/10.1146/annurev.fluid.40.111406.102224>
- Torres RR, Tsimplis MN (2011) Tides and long-term modulations in the Caribbean Sea. *Journal of Geophysical Research*. <https://doi.org/10.1029/2011jc006973>

Williams WG (1986) Lagrangian Measurements of Surface Circulation near Puerto Rico. *Journal of Physical Oceanography* 16:1715-1719. [https://doi.org/10.1175/1520-](https://doi.org/10.1175/1520-0485(1986)016<1715:lmoscn>2.0.co;2)

[0485\(1986\)016<1715:lmoscn>2.0.co;2](https://doi.org/10.1175/1520-0485(1986)016<1715:lmoscn>2.0.co;2)

Zetler BD, Cummings RA (1972) Tidal observations near an amphidrome. *Geophysical Surveys*

1:85–98. doi: 10.1007/bf01449552 <https://doi.org/10.1007/bf01449552>